

1

# 1 **Dual-targeted transcription factors are required for optimal** 2 **photosynthesis and stress responses in *Arabidopsis thaliana***

3 Piotr Gawroński<sup>1</sup>, Paweł Burdiak<sup>1</sup>, Lars B. Scharff<sup>2</sup>, Jakub Mielecki<sup>1</sup>, Magdalena  
4 Zaborowska<sup>1</sup>, Cezary Waszczak<sup>3</sup> and Stanisław Karpiński<sup>1\*</sup>

5 <sup>1</sup>Department of Plant Genetics, Breeding, and Biotechnology, Warsaw University of Life  
6 Sciences, 02-776 Warsaw, Poland

7 <sup>2</sup>Copenhagen Plant Science Center, Department of Plant and Environmental Sciences,  
8 University of Copenhagen, 1871 Frederiksberg C, Denmark

9 <sup>3</sup>Organismal and Evolutionary Biology Research Programme, Faculty of Biological and  
10 Environmental Sciences, and Viikki Plant Science Centre, University of Helsinki, 00014 Helsinki,  
11 Finland

12 **ORCID IDs:** 0000-0002-9773-3109 (P.G.); 0000-0003-0252-7116 (P.B.); 0000-0003-  
13 0210-3428 (L.B.S.); 0000-0003-1195-7118 (J.M.); 0000-0002-6550-0765 (M.Z.); 0000-0002-  
14 5978-7560 (C.W.); 0000-0002-4328-1207 (S.K.)

15 Correspondence to: Stanisław Karpiński: [stanislaw\\_karpinski@sggw.pl](mailto:stanislaw_karpinski@sggw.pl)



2

## 16 **Summary**

17 Chloroplast to nucleus retrograde signaling is essential for cell function, acclimation to  
 18 fluctuating environmental conditions, plant growth and development. The vast majority of  
 19 chloroplast proteins are nuclear-encoded and must be imported into the organelle after synthesis in  
 20 the cytoplasm. This import is essential for the development of fully functional chloroplasts. On the  
 21 other hand, functional chloroplasts act as sensors of environmental changes and can trigger  
 22 acclimatory responses that influence nuclear gene expression. Signaling *via* mobile transcription  
 23 factors (TFs) has been recently recognized as a way of communication between organelles and the  
 24 nucleus. In this study, we performed a targeted reverse genetic screen to identify novel dual-  
 25 localized TFs involved in chloroplast retrograde signaling during stress responses. We found that  
 26 CHLOROPLAST IMPORT APPARATUS 2 (CIA2), a TF with putative plastid transit peptide can  
 27 be detected in chloroplasts and the nucleus. Further, we found that CIA2, along with its homolog  
 28 CIA2-like (CIL) act in an unequally redundant manner and are involved in the regulation of  
 29 Arabidopsis responses to UV-AB, high light, and heat shock. Finally, our results suggest that both  
 30 CIA2 and CIL are crucial for chloroplast translation. Our results contribute to a deeper  
 31 understanding of signaling events in the chloroplast-nucleus cross-talk.

## 32 **Significance**

33 We found that a transcription factor CIA2 can be located in chloroplasts and nucleus. CIA2  
 34 and its close homolog CIL are involved in protein translation and abiotic stress responses, and we  
 35 suggest that they play an essential role in retrograde signaling between these organelles.

## 36 **Keywords**

37 Chloroplast retrograde signaling, CIA2, CIL, nonphotochemical quenching, photosynthesis,  
 38 thermo- and photooxidative stress tolerance, chloroplast translation



## 39 Introduction

40 In plants, intracellular communication between the nucleus, chloroplasts, and mitochondria is  
41 essential for the regulation and coordination of physiological processes such as growth,  
42 development, stress responses, photosynthesis, and respiration (de Souza *et al.*, 2017). Mechanisms  
43 that coordinate organellar and nuclear gene expression enable responses to fluctuating or rapidly  
44 changing environmental conditions.

45 Chloroplasts contain a few thousand proteins that are involved in photosynthesis, intracellular  
46 signaling, and biosynthesis of fatty acids, amino acids, hormones, vitamins, nucleotides, and  
47 secondary metabolites (Leister and Kleine, 2008). Most of these proteins are encoded by the nuclear  
48 genome, synthesized by cytosolic ribosomes, imported into the chloroplast, and targeted to a  
49 specific compartment within the chloroplast (Jarvis, 2008). Chloroplast genomes encode about 80  
50 of these proteins, most of which function in photosystems, photosynthetic electron transport, and  
51 the organellar gene expression machinery (Scharff and Bock, 2014; Daniell *et al.*, 2016).  
52 Consequently, dark and light reactions of photosynthesis—the function of the chloroplast—are  
53 strictly dependent on the interorganelle communication as the components of the photosynthetic  
54 apparatus are encoded by nuclear and plastid genomes, and a close cooperation between these two  
55 genomes is required for the development of functional chloroplasts and chloroplast plasticity (Jarvis  
56 and López-Juez, 2013).

57 The functionality of the photosynthetic apparatus depends on factors such as water and  
58 nutrient supply, light, and temperature (Gururani *et al.*, 2015). Besides photosynthesis, chloroplasts  
59 play an important role as redox sensors of environmental conditions and trigger acclimatory  
60 responses (Z., Li *et al.*, 2009). Changes in the developmental and metabolic states of chloroplasts or  
61 in the redox status of photosynthetic electron carriers can trigger alterations in the nuclear gene  
62 expression in a process called retrograde signaling (Chi *et al.*, 2013; Estavillo *et al.*, 2013; Guo *et al.*,  
63 2016). It is now well established that the perturbation of multiple plastid processes, including  
64 tetrapyrrole biosynthesis, protein synthesis, reactive oxygen species (ROS) metabolism, and dark  
65 and light reactions of photosynthesis, influences the expression of nuclear genes encoding  
66 photosynthetic proteins (Pesaresi *et al.*, 2006). Moreover, chloroplast retrograde signaling not only  
67 coordinates the expression of nuclear and chloroplast genes, which is essential for chloroplast  
68 biogenesis, but also ensures chloroplast vitality in changing environmental conditions (Barajas-  
69 López *et al.*, 2013) and triggers the expression of nuclear-encoded genes for other cellular  
70 compartments such as the cytoplasm and peroxisomes (Karpinski *et al.*, 1997; Karpiński *et al.*,  
71 1999; Mateo *et al.*, 2004; Mühlenbock *et al.*, 2008; Pogson *et al.*, 2008).

72 Changes in the absorbed light quality and intensity result in rapid changes in the redox state of  
73 photosynthetic electron carriers and lead to unbalanced production of ROS such as hydrogen



peroxide (H<sub>2</sub>O<sub>2</sub>), singlet oxygen, and superoxide anions (Karpiński *et al.*, 1999; Mullineaux *et al.*, 2006; Mühlenbock *et al.*, 2008; Pogson *et al.*, 2008). Recently, it was proposed that H<sub>2</sub>O<sub>2</sub> produced in chloroplasts can be directly transported to the nucleus to act as a signaling molecule as its accumulation in both compartments was observed immediately after exposure to light (Caplan *et al.*, 2015; Exposito-Rodriguez *et al.*, 2017). Moreover, H<sub>2</sub>O<sub>2</sub> produced in chloroplasts under drought and excessive light conditions influences the metabolism of 3'-phosphoadenosine 5'-phosphate (PAP), which, upon accumulation, modulates the expression of nuclear stress-responsive genes (Estavillo *et al.*, 2011; Chan *et al.*, 2016). Increased singlet oxygen generation in chloroplasts can also trigger specific retrograde signals. However, due to the high reactivity of singlet oxygen, its half-life is too short to enable direct transport to the nucleus, and it was proposed that carotenoid oxidation product, β-cyclocitral, acts as a stress signal induced by singlet oxygen produced in grana stacks (Ramel *et al.*, 2012). Moreover, singlet oxygen can be also produced in grana margins where it induces retrograde signaling through two plastid localized proteins, EXECUTER 1 and 2 (Lee *et al.*, 2007; Wang *et al.*, 2016; Dogra *et al.*, 2019).

In addition to signaling via ROS and metabolites, many transcription factors (TFs) were shown to be controlled by signals generated in the organelles. There are two known TFs, ANAC013 and ANAC017, which respond to the mitochondrial redox status (De Clercq *et al.*, 2013; Ng *et al.*, 2013). These TFs are anchored in the endoplasmic reticulum membrane, and in response to signals from mitochondrial complex III, they are released to the nucleus by the proteolytic cleavage of their transmembrane domains. After translocation to the nucleus, ANAC013 and ANAC017 regulate the expression of mitochondrial dysfunction stimulon genes (De Clercq *et al.*, 2013; Ng *et al.*, 2013). Further, it was recently shown that RADICAL-INDUCED CELL DEATH1 (RCD1) interacts with ANAC013 and ANAC017 to integrate ROS signals from chloroplasts and mitochondria (Shapiguzov *et al.*, 2019). Thus, the dual localization of TFs presents a possibility of their function in retrograde signaling.

Early, *in silico* analyses of Arabidopsis genes encoding putative TFs predicted targeting of at least 48 TFs to the plastids (Wagner and Pfannschmidt, 2006). Later, another *in silico*-based screen approach predicted that 78 Arabidopsis TFs reside in the plastids (Schwacke *et al.*, 2007). Indeed, several proteins exhibiting dual nuclear-plastid localization might potentially be involved in signal transduction pathways involving regulatory protein storage in the plastids. It was shown that most of the dual-targeted (nucleus and organelle) proteins have functions in the maintenance of DNA, telomere structuring, gene expression, or innate immunity (Krause *et al.*, 2012; Caplan *et al.*, 2015). These *in silico* studies were supported by *in vivo* evidence with WHIRLY1 being the first protein to be identified in the nucleus and plastids of the same plant cell (Grabowski *et al.*, 2008); however, its molecular function remains elusive. Later, the plant homeodomain (PHD) transcription factor PTM



5

(PHD-type TF with transmembrane domains) was shown to accumulate in the nucleus after release from the plastid surface. In the nucleus, PTM is thought to activate the transcription factor ABA INSENSITIVE 4 (ABI4), thereby providing a way to communicate the plastid status to the nucleus (Sun *et al.*, 2011). However, the roles of PTM and ABI4 in chloroplast-to-nucleus communication were recently questioned (Page *et al.*, 2017; Kacprzak *et al.*, 2019).

Although nuclear gene expression involves transcriptional control, it is generally believed that in the course of evolution, the regulation of plastid gene expression has shifted from predominantly transcriptional to predominantly posttranscriptional (Eberhard *et al.*, 2002), although significant transcriptional regulation occurs in chloroplasts (Liere and Börner, 2007). Posttranscriptional control is exerted at the level of mRNA stability and, most importantly, at the level of mRNA translation (Zoschke and Bock, 2018). During chloroplast biogenesis, translational regulation is required for the differentiation of chloroplasts from proplastids during the early development of stem and leaf tissues (Sugiura, 2014). At the later stages, in mature chloroplasts, translation is regulated mostly by light and controls chloroplast growth for division in the expanding cells of green tissues. Translational regulation also occurs in response to changing environmental conditions and quite often is essential to repair the photosynthesis machinery (Chotewutmontri and Barkan, 2018). For example, the regulation of *psbA* translation encoding for D1 core protein of photosystem II (PSII) is crucial for the repair of photodamaged PSII complexes, whereas the repression of *rbcL* translation encoding for a large subunit of RuBisCo occurs during oxidative stress (Nickelsen *et al.*, 2014).

In this paper, we aimed to characterize dual-localized TFs that can be involved in the communication between the chloroplast and the nucleus. As a result of a targeted reverse genetic screen, we focused on CHLOROPLAST IMPORT APPARATUS 2 (CIA2) and its homolog CIA2-like (CIL), which encode TFs with conserved *CONSTANS*, *CO-like*, and *TOC1* (CCT) domain at the C-terminus and putative plastid transit peptide at the N-terminus. Our results suggest that CIA2 and CIL play an important role in the regulation of chloroplast translation, thus influencing photosynthetic electron transport, accumulation of photosynthetic pigments, and chloroplast retrograde stress responses in *Arabidopsis thaliana*.

## 137 Results

### 138 Reverse genetic screen to identify chloroplast-targeted TFs involved in 139 retrograde signaling

140 Because chloroplast-to-nucleus signaling pathways are not sufficiently understood, we  
141 decided to use the targeted reverse genetic screen to identify new retrograde signaling components.



To this end, we focused on the identification of dual-localized TFs due to their potential role in chloroplast retrograde signaling (Sun *et al.*, 2011). To identify such TFs, we extracted and compared the gene identifiers obtained from three *Arabidopsis thaliana* plastid proteome databases (Schwacke *et al.*, 2003; Q., Sun *et al.*, 2009; Myouga *et al.*, 2013) and two transcription factor databases (Pérez-Rodríguez *et al.*, 2009; Jin *et al.*, 2014). This allowed us to identify a set of TFs with potential chloroplast localization. Further, we obtained T-DNA insertion lines for a selected set of genes (Data S1). These mutants were then subjected to conditions promoting chloroplast photooxidative stress, as we hypothesized that mutants lacking efficient communication between the chloroplast and the nucleus (possibly dependent on TFs) would show altered susceptibility to such treatments. During the primary screen, two types of stress treatments were applied: illumination with ultraviolet AB (UV-AB) and exposure to high light intensity in combination with cold (cHL). UV-AB significantly impairs photosynthetic electron transport and the general function of photosynthetic machinery (Hollósy, 2002; Caldwell, 1993). At the molecular level, UV-AB damages the ribosomes by crosslinking the cytosolic and chloroplast ribosomal proteins to RNA, thereby transiently inhibiting translation *in vivo* (Casati and Walbot, 2004; Ferreyra *et al.*, 2010). On the other hand, cHL causes imbalances in photosynthetic reactions resulting in the photoinhibition of photosystem II (PSII) and oxidative stress (Yabuta *et al.*, 2002; Distelbarth *et al.*, 2013). Most of the analyzed mutants were not affected by treatment with UV-AB and cHL as compared to Col-0 (Figure S1); however, based on the phenotypes of mutant lines, we could select eight candidate genes for further investigation (Table S1). Next, the coding sequences of six of the eight candidate genes were cloned, and fusion proteins with C-terminal YFP were expressed under the control of 35S promoter in *Arabidopsis* cotyledons to confirm their putative chloroplast localization (Figure S2 and Table S1). Except for p35S::AT5G57180:YFP, which showed chloroplast and nuclear localization, all the analyzed fusion proteins were found exclusively in the nucleus (Figure S2, Table S1). AT5G57180 encodes CHLOROPLAST IMPORT APPARATUS2 (CIA2) protein, which was previously found to play a role in protein import into chloroplasts (Sun *et al.*, 2001) and protein synthesis in chloroplasts (C.,-W., Sun *et al.*, 2009). In our reverse genetic screening (Figure 1a,b), line SALK\_045340 (hereafter referred to as *cia2-4*) that harbors T-DNA insertion in the first intron of the CIA2 gene (Figure 1c) showed increased susceptibility to UV-AB as indicated by the lower maximum efficiency of PSII ( $F_v/F_m$ ) and higher ion leakage resulting from the induction of cell death (Figure 1a). Similarly, the exposure to cHL reduced the  $F_v/F_m$  of *cia2-4* to a higher extent than that in the exposure to Col-0 (Figure 1b). The CIA2 protein contains a C-terminal conserved CCT motif, a characteristic feature of one family of TFs involved in light signal transduction (Strayer *et al.*, 2000). The CCT domain contains a putative nuclear localization signal (NLS), which is consistent with the nuclear localization of CIA2 observed earlier (Sun *et al.*, 2001).



177 However, our *in silico* analysis of CIA2 protein sequence predicted the existence of an N-terminal  
178 59 amino acid-long chloroplast transit peptide, which suggests that CIA2 can be imported into  
179 chloroplasts (Figure 1c and Data S1) (Schwacke *et al.*, 2003; Myouga *et al.*, 2013). The expression  
180 of full-length CIA2 fused with YFP (p35S::CIA2:YFP) resulted in a weak fluorescence signal; thus,  
181 we also expressed a 100 amino acid-long N-terminal part of CIA2 fused N-terminally to YFP  
182 (p35S::CIA2<sup>1-100</sup>:YFP). As a result, we observed a notably higher fluorescence intensity and  
183 confirmed the function of CIA2 transit peptide as the presence of fusion protein was detected in  
184 chloroplasts (Figure S2). Thus, based on the initial screen and protein localization experiments, we  
185 decided to focus on CIA2 that appears to be localized in the nucleus and chloroplast and is required  
186 for acclimatory responses to UV-AB and cHL.

## 187 CIA2 and CIL function redundantly

188 To confirm the role of *CIA2* under the analyzed stress conditions, we isolated two additional  
189 independent *cia2* mutant alleles, *cia2-2* (SALK\_004037, Col-0 background) and *cia2-3* (SGT49,  
190 Ler-0 background). In both mutants, the T-DNA was inserted into the first exon of *CIA2* (Figure  
191 1c). Because *cia2-4* is an intronic allele, we decided to focus our analysis on *cia2-2* and *cia2-3*  
192 alleles. To test whether the incorporation of T-DNA into the *CIA2* gene inhibits the accumulation of  
193 *CIA2* transcript, *cia2-2* and *cia2-3* mutants were subjected to quantitative RT-PCR analysis using  
194 two pairs of primers (Figure 1c,d and Figure S3d). Although we did not detect *CIA2* transcript in  
195 *cia2-2* using primers flanking the T-DNA insertion site, we detected the PCR product (although  
196 significantly lower than that in Col-0 and *cil-1*) using primers specific to 3'UTR of the *CIA2* gene  
197 suggesting the presence of truncated CIA2 transcript in *cia2-2* (Figure 1d). In *cia2-3*, we did not  
198 detect PCR products in both tested primer pairs (Figure S3d).

199 CIA2 shares 54% identical amino acids with CIA2-LIKE (CIL, AT4G25990); moreover, CIL  
200 also contains C-terminal CCT motif, N-terminal cTP and NLS (Figure 1c). Because of this  
201 sequence similarity, CIL was speculated to act redundantly to CIA2 (Sun *et al.*, 2001). To test this  
202 hypothesis, we isolated *cil-1* (SAIL\_228\_C01, Col-0 background) and *cil-2* (SK14786, Col-4  
203 background) mutants and introduced them into *cia2-2* background by crossing. Despite complete  
204 lack of *CIL* transcript in *cil-1* and *cil-2* mutants (Figure 1d and Figure S3a), both mutants were  
205 phenotypically indistinguishable from their corresponding wild-type (WT) plants. However, the  
206 double mutants *cia2-2 cil-1* and *cia2-2 cil-2* were paler than WT and the corresponding single  
207 mutants (Figure 1e and Figure S3b). To confirm visual differences, we measured the concentrations  
208 of photosynthetic pigments (Sumanta *et al.*, 2014). From this analysis, we deduced that the content  
209 of chlorophyll *a*, chlorophyll *b*, and total carotenoids is significantly lower in *cia2-2* and *cia2-3*  
210 (Figure 1f and Figure S3) mutants, thus supporting previous results obtained for *cia2-1* mutant (C.,-



211 W., Sun *et al.*, 2009). The introduction of *cil* mutations into *cia2-2* background further reduced the  
212 concentration of photosynthetic pigments (Figure 1e,f and Figure S3b,c), suggesting that CIA2 and  
213 CIL act in an unequally redundant manner.

214 To further confirm that the lack of CIA2 is responsible for the observed phenotype, we  
215 introduced constructs that encode CIA2:YFP and YFP:CIA2 fusion proteins under CIA2 native  
216 promoter and CIA2:YFP under 35S promoter into *cia2-2* background. The complementation lines  
217 pCIA2::*CIA2:YFP*<sub>*cia2-2*</sub> and pCIA2::*YFP:CIA2*<sub>*cia2-2*</sub> exhibited *CIA2* transcript level comparable to  
218 that of WT plants, whereas a ~7-fold increase was observed in p35S::*CIA2:YFP* plants (Figure 1g).  
219 The complementation and overexpression lines were visually indistinguishable from those of WT  
220 plants, and spectrophotometric measurement confirmed that the obtained transgenic lines had WT-  
221 like levels of photosynthetic pigments (Figure 1h). However, despite many efforts, we were unable  
222 to detect the YFP signal in these complementation lines, which might be related to the high  
223 proteolytic turnover rate of CIA2. Taken together, our results strongly suggest that CIA2 and CIL  
224 act redundantly and are required for the normal accumulation of photosynthetic pigments and thus  
225 for the proper functioning of photosystems and photosynthesis.

## 226 Characterization of *cia2 cil* responses in chloroplast-targeted stress

227 Because *cia2-4* mutant was initially selected from the screening using stress conditions that  
228 target the photosynthetic apparatus (Figure 1a,b), we set out to test the importance of *CIL* and *CIA2*  
229 under stress conditions using chlorophyll fluorescence as a readout. *cia2-4* was shown to be more  
230 susceptible to UV-AB that induced cell death (measured with ion leakage and chlorophyll  
231 fluorescence) to a significantly higher extent than in Col-0 plants (Figure 1a). In agreement with  
232 these data, the exposure of *cia2-2* mutant to UV-AB resulted in similar changes in the  
233 photosynthetic parameters, which were significantly affected 1 and 2 days after the treatment  
234 (Figure 2a-c). Moreover, the introduction of *cil* mutant into *cia2-2* intensified the effect (Figure 2  
235 and Figure S4). Measurements of ion leakage after UV-AB treatment confirmed chlorophyll  
236 fluorescence observations suggesting increased cell death in *cia2-2* and even stronger effect in  
237 *cia2-2 cil-1* and *cia2-2 cil-2* (Figure 2 and Figure S4).

238 To confirm the role of CIA2, and test whether CIL is required for the high light response, we  
239 exposed the plants to blue HL (bHL) and monitored  $F_v/F_m$  (Figure 3 and Figure S4). At all tested  
240 time points, we observed stronger photoinhibition of PSII as evidenced by decreased  $F_v/F_m$  in *cia2-2*  
241 *cil-1* and *cia2-2 cil-2* (compared to that in WT plants) measured at a level of whole rosette with  
242 the strongest effect visible in young (not fully developed) leaves (Figure 3a,b and Figure S4e). As  
243 increased photoinhibition can result from either increased damage of PSII or decreased PSII repair  
244 (Miyata *et al.*, 2015), we monitored recovery after exposure to bHL (Figure 3c). We did not observe



245 differences between Col-0 and *cia2-2 cil-1* in the rate of  $F_v/F_m$  recovery suggesting that increased  
 246 susceptibility to bHL in *cia2-2 cil-1* is not related to the repair of PSII but to increased damage.  
 247 HL-induced damage of the photosynthetic electron transport chain is often related to the production  
 248 of ROS such as singlet oxygen, which is mainly produced in PSII antenna, and superoxide anion  
 249 and  $H_2O_2$ , which are mainly produced in the vicinity of PSI (Smirnoff and Arnaud, 2019). To  
 250 simulate conditions of photoinhibition at the PSII side and induce overproduction of ROS, we  
 251 treated leaf disks of Col-0 and *cia2-2 cil-1* with 3-(3,4-dichlorophenyl)-1,1-dimethylurea (DCMU)  
 252 and methyl viologen (MV) and monitored  $F_v/F_m$  (Figure 3d). DCMU noncovalently binds to the  
 253 quinone B binding side of PSII and inhibits the photosynthetic electron transfer to the plastoquinone  
 254 (PQ) pool, thus keeping reduced quinone A and oxidized PQ pool. MV is able to induce the  
 255 accumulation of superoxide anion in chloroplast stroma. Upon DCMU and MV treatments,  $F_v/F_m$   
 256 significantly more decreased in *cia2-2 cil-1* than in Col-0, suggesting that the double mutant is  
 257 more susceptible to photoinhibition and ROS such as singlet oxygen and  $H_2O_2$  (Figure 3d).  
 258 Collectively, our results suggest that CIA2 and CIL are required for an adequate response to  
 259 conditions that promote photooxidative stress in chloroplasts and trigger cell death signaling.

## 260 Role of CIA2 and CIL in the regulation of photosynthesis and NPQ

261 Increased susceptibility to HL and UV-AB can be a consequence of impaired  
 262 nonphotochemical quenching (NPQ), which is responsible for the dissipation of excess light energy  
 263 as heat (Kulasek *et al.*, 2016; Białasek *et al.*, 2017). Thus, we monitored NPQ using chlorophyll *a*  
 264 fluorescence in Col-0, *cia2-2*, *cil-1*, *cil-2*, *cia2-2 cil-1*, and *cia2-2 cil-2* (Figure 4 and Figure S5).  
 265 We observed that NPQ was slightly (but statistically significant) decreased in *cia2-2 cil-1* and  
 266 *cia2-2 cil-2* at a level of the whole rosette. Differences were more pronounced when only young,  
 267 not fully developed leaves were analyzed. In young leaves of *cia2-2 cil-1*, NPQ was decreased by  
 268 40% when compared to Col-0 (Figure 4a,b). It is well established that the process of NPQ is  
 269 controlled by a small PSII protein PsbS, which is activated by the acidification of the thylakoid  
 270 lumen (Niyogi *et al.*, 2005). To check whether this process is impaired in *cia2 cil* mutants, we  
 271 measured the proton gradient ( $\Delta pH$ ) and electric potential ( $\Delta\psi$ ), which constitute proton motive  
 272 force (PMF) (Figure 4c-e and Figure S5c-e) at two actinic light intensities (i.e., 160 and 660  $\mu mol$   
 273  $m^{-2} s^{-1}$ ). Although we did not observe differences in PMF between the analyzed genotypes, we noted  
 274 that  $\Delta pH$  in *cia2-2* as well as in *cia2-2 cil-1* and *cia2-2 cil-2* was significantly decreased as  
 275 compared to that in Col-0 (Figure 4e and Figure S5e), which correlates well with decreased NPQ in  
 276 these genotypes. Because the rosette size of *cia2-2 cil-1* was slightly smaller than that of Col-0  
 277 (Figure 1d, Figure 4b), we also measured  $CO_2$  assimilation as a function of light intensity (20–2000  
 278  $\mu mol m^{-2} s^{-1}$ ) and  $CO_2$  concentration (20–1500 ppm) (Figure 4f,g) and observed moderate but



10

279 statistically significant decrease in CO<sub>2</sub> assimilation in *cia2-2 cil-1* within the tested range of light  
280 intensity and CO<sub>2</sub> concentration. Taken together, our results strongly suggest that CIA2 and CIL are  
281 required for optimal NPQ and proper formation of trans-thylakoid proton gradient as well as for  
282 optimal CO<sub>2</sub> assimilation.

## 283 Chloroplast translation is attenuated in *cia2 cil*

284 It was shown that CIA2 binds to the promoters of genes encoding the chloroplast ribosomal  
285 proteins, and decreased expression of these genes was observed in *cia2-1* mutant (Sun *et al.*, 2001).  
286 To check whether a similar phenomenon was observed in *cia2-2* and if the expression of these  
287 genes was dependent on the activity of CIL, we checked the expression of *Rps6*, *Rpl11*, *Rpl18*, and  
288 *Rpl28* nuclear genes encoding for bS6c, uL11c, uL18c, and bL28c chloroplast ribosomal proteins  
289 using qRT-PCR (Figure 5a). The expression of all analyzed genes was decreased in *cia2-2* as  
290 compared to that in Col-0 and *cil-1*. The introduction of *cil-1* mutation into *cia2-2* led to stronger  
291 reduction in the expression of all genes except *Rpl18*, whose transcript was at the same level as that  
292 in *cia2-2* (Figure 5a). To gain more comprehensive view of gene expression changes, we performed  
293 whole transcriptome sequencing (RNA-seq) for Col-0, *cia2-2*, *cil-1*, and *cia2-2 cil-1* plants. First,  
294 we focused on genes encoding for proteins involved in chloroplast translation. Our analysis  
295 revealed that the expression of 21 out of 66 chloroplast ribosome genes is inhibited in *cia2-2 cil-1*  
296 (Figure 5b) including two genes encoded by the chloroplast genome (i.e., *rpl2* and *rpl32*, encoding  
297 for the ribosomal proteins uL2c and bL32c). Pentatricopeptide repeat (PPR) proteins are involved in  
298 every step of chloroplast gene expression, namely transcription, RNA metabolism, and translation  
299 (Barkan and Small 2014). Thus, we checked the expression of chloroplast-targeted PPRs in *cia2-2*  
300 *cil-1* and found 13 down- and 7 upregulated PPR genes (Figure 5b). Further, the expression analysis  
301 of other genes possibly involved in plastid translation revealed the presence of both up- and  
302 downregulated genes (Figure 5b). Taken together, the transcriptome profiling indicates that the lack  
303 of CIA2 and CIL leads to altered expression of multiple genes encoding the components of the  
304 chloroplast translation machinery.

305 To further confirm that CIA2 and CIL are required for optimal chloroplast translation, we  
306 subjected Col-0 and *cia2-2 cil-1* to polysome loading assays. We examined the ribosomal loading  
307 of *psbD* mRNA (encoding for the D2 protein of PSII) using sucrose gradient fractionation followed  
308 by northern blot analysis (Figure 5c). This analysis showed that *psbD* mRNA was underrepresented  
309 in the polysomal fractions in *cia2-2 cil-1* compared to that in Col-0, and the mRNA was shifted  
310 toward lighter (monosome) fractions, suggesting that *psbD* mRNA was associated with fewer  
311 ribosomes and that its translation was reduced in *cia2-2 cil-1*. Further, as multiple lines of evidence  
312 indicate that CIA2 and CIL are involved in chloroplast translation, we also tested the growth of Col-



11

0, *cia2-2*, *cil-1*, and *cia2-2 cil-1* in media supplemented with spectinomycin, which inhibits this process. Spectinomycin binds the 30S subunit of the 70S ribosome and prevents translocation of peptidyl-tRNA from A to P site; consequently, many Arabidopsis translation mutants showed increased susceptibility to this antibiotic (Parker *et al.*, 2014). In agreement with the results of ribosome loading experiments, we observed severe inhibition of pigment accumulation in *cia2-2 cil-1* grown in media supplemented with spectinomycin (Figure 5d), which suggests that CIA2 and CIL play a role in plastid translation.

The decreased chlorophyll content in young leaves and inhibited translation in *cia2-2 cil-1* led us to analyze chloroplast ribosomal RNA (rRNA) maturation. In Arabidopsis chloroplasts, all rRNAs are encoded by the polycistronic *rrn* operon (Bollenbach *et al.*, 2007). Upon processing of the initial transcript by distinct endo- and exonucleases, tRNAs, precursors of 16S and 5S rRNAs and bicistronic 23S-4.5S intermediate are created (Figure 6a). The 23S-4.5S precursor is cut to produce 4.5S and 23S rRNA fragments. The maturation of 23S rRNA is followed by the introduction of two gaps ("hidden breaks") producing three distinct parts of 0.4, 1.1, and 1.3 kb; however, the functional relevance of this postmaturation processing is not clear (Bollenbach *et al.*, 2007; Fristedt *et al.*, 2014). The capillary electrophoresis of RNA isolated from young leaves showed that 1.1 and 1.3 kb species of 23S rRNA and 16S rRNA accumulate to lower level in *cia2-2* and *cia2-2 cil-1* mutants as compared to that in WT plants (Figure 6b). These results suggest that the expression and/or processing of 16S and 23S rRNAs are dependent on CIA2 and CIL. To further characterize rRNA maturation, we performed northern blot analysis with probes specific to *rrn16* and *rrn23* (Figure 6c). We observed only slightly lower level of 16S rRNA in *cia2-2 cil-1* without accumulation of its 1.7 kb precursor suggesting that the processing of *rrn16* is not impaired (Figure 6c). In agreement with the results of capillary electrophoresis, we observed decreased accumulation of 0.4, 1.1, 1.3, and 1.7 kb species and increased accumulation of 2.4 kb fragment of 23S rRNA in *cia2-2 cil-1* (Figure 6c). These results suggest that gap incorporation between 1.1 kb and 1.3 kb fragments is less efficient in *cia2-2 cil-1* mutant. To confirm these results, we performed qRT-PCR analysis with primers spanning hidden breaks (Figure 6d) and obtained confirmatory results.

Next, we tested whether the perturbations of chloroplast translation are linked to the decreased NPQ observed in *cia2 cil* (Figures 4f and S6). For this, we measured NPQ in well-characterized chloroplast translation mutants *prpl1-1*, *prps1-1*, *psrp5-R1*, and *rps17-1* (Pesaresi *et al.*, 2001; Romani *et al.*, 2012; Tiller *et al.*, 2012; Tadini *et al.*, 2016) (Figure S6). However, in contrast to *cia2 cil*, NPQ in these mutants was increased as compared to that in Col-0 plants (Figure S6). These results suggest that the observed decrease in NPQ in *cia2 cil* mutant is not related to inhibited chloroplast translation. Taken together, our results suggest that the translation of



12

348 chloroplast mRNA and the maturation and accumulation of 23S rRNA are influenced by CIA2 and  
349 CIL.

## 350 Lack of CIA2 and CIL confers heat stress tolerance

351 To our surprise, RNA-seq analysis showed that many genes induced in *cia2-2 cil-1* were  
352 annotated as heat shock proteins (HSPs) (Data S2). Further, the gene ontology (GO) enrichment  
353 analysis demonstrated that GO terms related to heat response and acclimation were overrepresented  
354 among genes induced in *cia2-2 cil-1* (Figure 7a). To confirm the RNA-seq results, we performed  
355 qRT-PCR analysis to assess the transcript level of *HEAT SHOCK TRANSCRIPTION FACTOR A2*  
356 (*HSFA2*) and *HEAT SHOCK PROTEIN 70-4* (*HSP70-4*) in *cia2-2*, *cia2-3*, *cil-1*, *cia2-2 cil-1*, and  
357 corresponding WT plants (Figure 7b). Our results confirmed strong induction of both genes in *cia2*  
358 mutants, and even stronger induction was observed in *cia2-2 cil-1* double mutant (Figure 7b). To  
359 check whether increased expression of many HSPs can confer thermotolerance, we grew *cia2-2*,  
360 *cil-1*, *cia2-2 cil-1*, and Col-0 seedlings on Petri dishes and exposed them to heat stress (45 °C) for  
361 20–40 min (Figure 7c,d). Exposure to 45 °C for 30 min resulted in almost complete bleaching and  
362 growth inhibition of Col-0 plants (Figure 7c). A similar phenotype was observed in the case of  
363 *cia2-2* and *cil-1* mutants; however, *cia2-2 cil-1* plants were affected to a significantly lower extent,  
364 and nearly all individuals retained cotyledon and leaf pigmentation (Figure 7c,d). Furthermore, at  
365 other tested time points, *cia2-2 cil-1* was more resistant to heat stress than the remaining genotypes  
366 (Figure 7c,d). These results suggest that CIA2 and CIL are redundantly involved in the modulation  
367 of thermotolerance presumably through the regulation of HSP expression.

## 368 Discussion

369 Mature chloroplasts contain approximately 3000 proteins, the majority of which are located in  
370 the stroma and thylakoid membranes (Jarvis and Robinson, 2004). Chloroplasts are capable of  
371 semiautonomous protein synthesis; however, their genomes encode only approximately 80 proteins.  
372 More than 95% of their proteins are products of the nuclear genome, which are translated in the  
373 cytosol and then imported (Jarvis and Robinson, 2004). Plastid biogenesis and maintenance depend  
374 on the coordinated assembly of proteins imported from the cytosol with proteins translated within  
375 plastids (Jarvis and López-Juez, 2013). Chloroplasts in leaf cells have a greater need for protein  
376 import and protein synthesis than plastids in other organs due to a large number of proteins required  
377 for photosynthesis (Jarvis and Robinson, 2004). Nuclear-encoded proteins are transported across the  
378 double chloroplast membrane due to the activity of a specialized translocon complex (Nakai, 2015;  
379 Paila *et al.*, 2015). This mechanism is essential for chloroplast biogenesis and requires coordinated  
380 action of multiple proteins. Previous reports revealed a positive regulatory effect of CIA2 on the



transcription of the translocon genes Toc33 and Toc75 in leaves (Sun *et al.*, 2001; C.-W., Sun *et al.*, 2009), suggesting the role of CIA2 in protein import into the chloroplast.

In the present study, we found that CIA2 has a functional cTP which, in transient expression experiments, targets a fraction of CIA2:YFP fusion protein to chloroplasts of Arabidopsis seedlings (Figure 1c, Figure S2). In agreement with our observation, recently characterized barley (*Hordeum vulgare*) CIA2 homolog, HvCMF7, was also shown to be localized in chloroplasts (Li *et al.*, 2019). In the first attempt to determine the subcellular localization of CIA2, the GUS:CIA2 fusion protein was found to reside exclusively in the nucleus (Sun *et al.*, 2001). We speculate that the discrepancy between our data and the previous work might be related to the masking of CIA2 cTP by the GUS fused to CIA2 N-terminus, thus inhibiting the import of GUS:CIA2 fusion protein into chloroplasts (Sun *et al.*, 2001). From the results of our complementation test, we were unable to determine the significance of CIA2 chloroplast localization because the expression of both constructs, pCIA2::CIA2:YFP and pCIA2::YFP:CIA2, restored the accumulation of photosynthetic pigments in *cia2-2* mutant (Figure 1h). Thus, we speculate that at least with regard to the determination of the levels of photosynthetic pigments, the chloroplast localization of CIA2 is not crucial. Interestingly, despite clear complementation effect and restoration of CIA2 transcript level, we did not observe YFP signal in stable transformants expressing CIA2:YFP fusion either under native or 35S promoter, suggesting that the CIA2 protein level might be subject to strict posttranslational control. A similar scenario was observed for ABI4 (Finkelstein *et al.*, 2011) and RCD1 (Jaspers *et al.*, 2009), suggesting that certain regulatory proteins might be unstable and/or degraded by the proteasome thus preventing their detection in standard conditions. A comparable phenomenon was observed in the case of another key player of retrograde signaling, GUN1, which accumulates in chloroplasts only at a very early stage of leaf development (Wu *et al.*, 2018).

Inefficient chloroplast protein import causes cytosolic overaccumulation of preproteins, which results in the activation of chaperones such as HSP70 and HSP90, which were recently postulated to be key components of the chloroplast retrograde signaling pathway (Wu *et al.*, 2019). Accordingly, we observed strong transcriptional induction of cytosolic chaperones and increased thermotolerance in *cia2 cil* mutant (Figure 7). On the other hand, it was demonstrated that thermotolerance is regulated by chloroplast signals that depend on the redox state of the PQ pool or hydrogen peroxide produced in chloroplasts (Dickinson *et al.*, 2018).

The redox state of the PQ pool and H<sub>2</sub>O<sub>2</sub> are also involved in high-light acclimatory responses (Karpinski *et al.*, 1999; Mühlenbock *et al.*, 2008; Gilroy *et al.*, 2016). Experimentally, it is almost impossible to separate foliar heat shock from high-light responses, because exposure to high light for a few seconds significantly warms up Arabidopsis leaves due to the dissipation of energy as heat (Kulasek *et al.*, 2016). Therefore, it is interesting that CIA2 and CIL antagonistically influence



high-light and UV-B acclimation *versus* thermotolerance in ambient light. Abolished expression of *CIA2* and *CIL* genes in double mutant causes growth reduction, acclimation, and photosynthesis dysfunction, while it can cause thermotolerance expressed as seedling survival rate at high temperatures. However, we were not able to identify the precise role of *CIA2* and *CIL* in the antagonistic regulation of these processes, and we plan to perform field experiments similar to those we did for cell death conditional regulators (i.e. *LSD1*, *EDS1*, *PAD4*) (Wituszyńska *et al.*, 2013). These proteins, depending on growing conditions, differently regulate chloroplast retrograde cell death signaling for growth, photosynthesis, high-light and UV-B acclimation, water use efficiency, and seed yield (Wituszyńska *et al.*, 2013; Wituszyńska *et al.*, 2015; Bernacki *et al.*, 2019).

Our data show that *CIA2* and its close homolog *CIL* play a relevant function in the chloroplast biogenesis process (Figure 1). The *cia2 cil* double mutant exhibited a pale green phenotype, which was much more pronounced than that observed in single *cia2* mutants, suggesting that these proteins act in an unequally redundant manner. Double mutant plants displayed a significantly lower concentration of chlorophyll *a*, chlorophyll *b*, and carotenoids (Figure 1 and Figure S3), suggesting impairment in the conversion of light into chemical energy. A similar phenotype was observed in plants lacking the activity of Golden 2-like (GLK) transcription factors. In the nuclear genome, GLKs are involved in the related expression of nuclear chloroplast-localized proteins and photosynthesis-related genes in *Zea mays*, *Physcomitrella patens*, and *Arabidopsis thaliana* (Yasumura *et al.*, 2005; Waters *et al.*, 2009). Like *cia2 cil*, the *glk1 glk2* double mutants were pale green and deficient in the formation of the photosynthetic apparatus (Waters *et al.*, 2009). Our RNA-seq and qRT-PCR-based expression data revealed a significant transcriptional downregulation of chloroplast ribosome genes in *cia2 cil* plants. Almost one-third of 66 chloroplast ribosome protein genes were significantly repressed in *cia2-2 cil-1*. These data are consistent with previous reports showing that *CIA2* binds to the promoters of genes encoding chloroplast ribosomal proteins (C.,-W., Sun *et al.*, 2009) and support a positive regulatory role of *CIA2* in chloroplast translation. Chloroplast ribosomal proteins are encoded by both nuclear and chloroplast genomes (Zoschke and Bock, 2018). Interestingly, the majority of ribosomal genes downregulated in *cia cil* are nuclear-encoded, which, together with partial chloroplast localization of *CIA2* (Figure S2), suggests that *CIA2* and *CIL* might act as chloroplast sensors of the environmental stimuli and mediate chloroplast-dependent adaptive responses (Estavillo *et al.*, 2013), and the dual chloroplast/nuclear localization of *CIA2* (Figure S2) supports its involvement in this process.

Finally, our data indicate that *CIA2* and *CIL* influence chloroplast translation by the regulation of ribosome assembly and maturation as *cia2 cil* double mutants displayed a disturbed accumulation of 23S rRNA (Figure 6). In plant chloroplasts, 23S rRNA constitutes a component of a large (50S) subunit of chloroplast ribosomes. The rRNA undergoes postmaturation processing,



15

451 which includes a site-specific cleavage that generates gapped, discontinuous rRNA molecules  
 452 (Nishimura *et al.*, 2010). The maturation process is followed by the removal of a specific region and  
 453 introduction of a gap (the so-called hidden break) into the 23S rRNA (Bollenbach *et al.*, 2005). This  
 454 molecule is split into four major fragments of 1.7, 1.3, 1.1, and 0.4 kb. Chloroplasts of all  
 455 dicotyledonous plants have hidden breaks at similar locations. Several proteins have been reported  
 456 to bind to a 23S rRNA segment close to the hidden break sites (Bieri *et al.*, 2017). We observed an  
 457 increased accumulation of the 2.4 kb 23S rRNA species and a reduced occurrence of the hidden  
 458 break in this species (Figure 6c,d). Interestingly, the expression of the two genes *Rpl19.1* and  
 459 *Rpl19.2* (Figure 5b), which encode for the ribosomal protein bL19c binding close to the hidden  
 460 break (Bieri *et al.*, 2017), was reduced. This indicates that the lack of bL19c could influence the  
 461 rRNA structure in a way that makes it less susceptible to the hidden break incorporation. The lack  
 462 of bL19c could be one of the causes of the impaired biogenesis of the 50S subunit as shown by the  
 463 reduced accumulation of the 23S rRNA (Figure 6c,d). The deficiencies in rRNA maturation  
 464 observed in *cia2-2 cil-1* double mutant suggest that CIA and CIL might play a role in this process,  
 465 either directly by binding and processing 23S rRNA precursor or more likely indirectly by  
 466 regulating the expression of ribosomal proteins.

467 In conclusion, the presented results demonstrate high complexity and elegance of chloroplast  
 468 retrograde signaling and anterograde nuclear responses that depend on putative TFs such as CIA2  
 469 and CIL. This complexity is not only observed on the molecular and biochemical levels but also on  
 470 the physiological level of acclimatory responses as well as on the regulation of chloroplast  
 471 biogenesis and plant growth and development. To better understand the interdependence of these  
 472 regulatory processes, further interdisciplinary studies on the function of these proteins are needed.

## 473 **Experimental procedures**

### 474 **Plant material and growth conditions**

475 *Arabidopsis thaliana* ecotypes Columbia-0 (Col-0), Columbia-4 (Col-4), and Landsberg  
 476 erecta (Ler-0) were used as controls for analyzed mutants. *cia2-2* (SALK\_004037), *cia2-3*  
 477 (SGT49), *cia2-4* (SALK\_045340), *cil-1* (SAIL\_228\_C01), and *cil-2* (SK14786) were ordered from  
 478 the Nottingham Arabidopsis Stock Centre (NASC) and genotyped using primers shown in Table  
 479 S2. The *cia2-2 cil-1* and *cia2-2 cil-2* double mutants were generated by crossing. Plants were  
 480 grown on Jiffy pots (Jiffy Products) for 3–4 weeks in a growing chamber in long-day photoperiod  
 481 (16 h/8 h) under constant white light of 140–160  $\mu\text{mol photons m}^{-2} \text{s}^{-1}$  at 22 °C.



16

## 482 Databases

483 In this work, we used information extracted from proteome databases to identify chloroplast  
484 proteins [Plant Proteomics Database at Cornell (<http://ppdb.tc.cornell.edu/>) (Q., Sun *et al.*, 2009);  
485 The Chloroplast Function Database II (<http://range-v2.psc.riken.jp/chloroplast/>) (Myouga *et al.*,  
486 2013), and ARAMEMNON (<http://aramemnon.uni-koeln.de>) (Schwacke *et al.*, 2003)] and TF  
487 databases to look for annotated TFs in Arabidopsis [The Plant Transcription Factor Database ([http://](http://plntfdb.bio.uni-potsdam.de)  
488 [plntfdb.bio.uni-potsdam.de](http://plntfdb.bio.uni-potsdam.de)) (Pérez-Rodríguez *et al.*, 2009) and PlantTFDB  
489 (<http://planttfdb.cbi.pku.edu.cn/>) (Jin *et al.*, 2014)].

## 490 Vector constructions and Arabidopsis transformation

491 *CIA2* and *CIL* full CDSs were amplified with primers listed in Table S2 by PCR using cDNA  
492 from Col-0 plants. PCR products of expected length were purified from agarose gel and inserted  
493 into the entry clone using the pENTR/D-TOPO cloning kit (Invitrogen). DNA fragments encoding  
494 for N-terminal 100 aa as well as predicted cTP were amplified from plasmids carrying *CIA2* and  
495 *CIL* CDSs. Next, they were subcloned into pGWB641 vector (Nakagawa *et al.*, 2007) using  
496 Gateway® LR Clonase™ II enzyme mix (Invitrogen). These constructs were introduced into  
497 *Agrobacterium fabrum* (GV3101). The vector was transformed into Col-0 and/or *cia2-2* mutant by  
498 the floral dip method. The T3 generation of homozygous transgenic plants was obtained and used  
499 for further experiments. The complementation lines were obtained in a similar manner, but in the  
500 final step, the promoter, CDS and YFP sequences were cloned into the pK7m34GW binary vector  
501 and transformed into *Agrobacterium*.

502 In parallel, whole *CIA2* and the *CIA2* fragment encoding for the 100 aa N-terminal part of  
503 *CIA2* were amplified from cDNA using USER compatible (Nour-Eldin *et al.*, 2006) primers and the  
504 improved Pfu X7 polymerase (Nørholm, 2010). PCR fragments were cloned into the pLIFE001  
505 vector (Silvestro *et al.*, 2013) and introduced into *Agrobacterium* (GV3101) for transient expression  
506 in Arabidopsis seedlings and subcellular localization using the FAST method (J., F., Li *et al.*, 2009).

## 507 Chlorophyll *a* fluorescence, CO<sub>2</sub> assimilation, and ΔpH measurements

508 Chlorophyll *a* fluorescence parameters were measured in dark-acclimated (30 min) plants  
509 using PAM FluorCam 800 MF PSI device (Brno, Czech Republic) as described earlier (Gawronski  
510 *et al.*, 2014). CO<sub>2</sub> assimilation was measured as described earlier (Burdiak *et al.*, 2015). The  
511 electrochromic pigment shift (ECS) was measured using DUAL-PAM 100 equipped with P515/535  
512 module (Walz), which allows the simultaneous measurement of the dual beam 550–515 nm signal  
513 difference (Schreiber and Klughammer, 2008). Before measurement, the plants were dark



17

514 acclimated for 30 min and subsequently illuminated with red actinic light of 160  $\mu\text{mol photons m}^{-2}$   
 515  $\text{s}^{-1}$  for 20 min. At the beginning of each measurement, the actinic light was turned off for 23 s, and  
 516 three single turnover (ST) flashes were applied. Next, the red actinic light (160  $\mu\text{mol photons m}^{-2} \text{s}^{-1}$ )  
 517 was turned on, and after 4 min, it was again turned off to determine total ECS,  $\Delta\text{pH}$ , and  $\Delta\Psi$  as  
 518 described previously (Herdean *et al.*, 2016). Immediately after the first measurement, the ECS  
 519 signal was recorded using the same protocol but at a higher actinic light intensity (660  $\mu\text{mol}$   
 520  $\text{photons m}^{-2} \text{s}^{-1}$ ). The ECS signal was normalized to the highest ST peak recorded at the beginning  
 521 of each measurement.

## 522 Photosynthetic pigment analysis

523 For pigment analysis, approximately 15–20 mg of tissue was collected from the sixth leaf of  
 524 3–4-week-old plants. Tissue was immediately frozen in liquid nitrogen and ground in the presence  
 525 of methanol. Absorbance was measured using Multiskan GO (Thermo Fisher Scientific)  
 526 spectrophotometer after the clarification of the supernatant by centrifugation. Photosynthetic  
 527 pigment concentrations were calculated as reported previously (Sumanta *et al.*, 2014).

## 528 Stress treatments and ion leakage

529 High-light stress was applied to whole plants using blue light (455 nm) of 1100  $\mu\text{mol photons}$   
 530  $\text{m}^{-2} \text{s}^{-1}$  for the indicated time. As a light source, SL3500-B-D LED array was used (PSI, Brno, Czech  
 531 Republic). After illumination, the plants were dark acclimated for 20 min, and chlorophyll *a*  
 532 fluorescence was measured as described above. For recovery experiments, we used blue light of  
 533 2500  $\text{photons m}^{-2} \text{s}^{-1}$  for 2.5 h. After this treatment, the plants were placed in the growing chamber  
 534 for an indicated period of time followed by 20 min dark acclimation and chlorophyll *a* fluorescence  
 535 measurement. For UV-AB stress, UVC 500 Crosslinker (Hoefer Pharmacia Biotech, USA)  
 536 equipped with UV-A (TL8WBLB, Philips) and UV-B lamps (G8T5E, Sankyo Denki) was  
 537 employed. The plants were exposed to single UV-AB episode at a dose of 800  $\text{mJ cm}^{-2}$ , and  
 538 chlorophyll *a* fluorescence was analyzed 24 and 48 h after stress. Ion leakage was also used to  
 539 analyze cell death 48 h after UV-AB stress as described before (Burdiak *et al.*, 2015) with the  
 540 following modification: total ion leakage was evaluated after freezing at  $-80^\circ\text{C}$  overnight.

## 541 Herbicide treatments

542 Leaf disks cut from 4-to 5-week-old plants were treated with 62.5  $\mu\text{M}$  of 3-(3,4  
 543 dichlorophenyl)-1,1-dimethylurea (DCMU) and 5  $\mu\text{M}$  of N,N'-dimethyl-4,4'-bipyridinium  
 544 dichloride (methyl viologen, MV) with 0.05% Tween-20 and were kept in the growing chamber  
 545 under ambient light between measurements. The maximum efficiency of PSII ( $F_v'/F_m'$ ) of leaf disks



18

546 was measured using FluorCam 800MF (Photon Systems Instruments, Czech Republic). As a  
547 control, we used leaf disks incubated in identical conditions without herbicides.

## 548 RNA isolation and transcriptome profiling

549 For RNA isolation, only young (not fully developed) leaves were used. In the middle of the  
550 photoperiod, the leaves were detached and frozen in liquid nitrogen. For HL treatment, whole  
551 rosettes were illuminated with blue light (length 1100  $\mu\text{mol photons m}^{-2} \text{ s}^{-1}$ ) for 1 h. Immediately  
552 following the treatment, young leaves were detached and frozen in liquid nitrogen. Leaf samples  
553 represent three biological replicates, and each contained leaves from at least three individual plants.  
554 Frozen leaves were ground using mortar and pestle in liquid nitrogen, and RNA was isolated using  
555 Spectrum™ Plant Total RNA Kit (Sigma). The quality and quantity of total RNA were evaluated  
556 using Experion™ StdSens RNA Kit (Bio-Rad), and the samples with RQI value higher than 9.0  
557 were used for RNA-seq library construction using TruSeq RNA Sample Prep Kit v2 (Illumina).  
558 RNA-seq libraries were sequenced in 100 bp paired-end reads using Illumina HiSeq 4000. RNA-seq  
559 library preparation and sequencing were conducted by Macrogen (Seoul, Korea). Reads were  
560 pseudomapped to *Arabidopsis thaliana* cDNAs (Ensembl, TAIR 10, release 35) using Salmon  
561 software (Patro *et al.*, 2017). Transcript-level abundances were imported into R using tximport  
562 (Soneson *et al.*, 2016) and analyzed using DESeq2 package (Love *et al.*, 2014). Significantly  
563 enriched GO terms were identified in up-/downregulated gene sets using PANTHER Classification  
564 System at <http://geneontology.org/>.

## 565 Availability of supporting data

566 RNA-seq data are provided at (uploaded upon manuscript acceptance).

## 567 Quantitative real-time PCR

568 RNA for qRT-PCR was isolated as described above. RNA was treated with DNase (TURBO  
569 DNA-free™ Kit, Thermo Fisher Scientific) to remove residual DNA. Next, cDNA was synthesized  
570 from 1  $\mu\text{g}$  of total RNA using High-Capacity cDNA Reverse Transcription Kit (Applied  
571 Biosystems). PCRs were run on a 7500 Fast Real-Time PCR System (Applied Biosystems) using  
572 PerfeCTa™ SYBR® Green FastMix™, Low ROX™ (Quanta BioSciences) according to the  
573 manufacturer's instructions. All primers used in qRT-PCR are listed in Table S2. The amplification  
574 efficiency of primers was calculated on the basis of the amplification curve using LinRegPCR  
575 software (Ramakers *et al.*, 2003). Relative expression was calculated using EasyqpcR package  
576 (<http://www.bioconductor.org/packages/release/bioc/html/EasyqpcR.html>) with *PP2AA3* and  
577 *TIP41L* as reference genes.



19

## 578 Northern blot and polysome analysis

579 Northern blot analysis and polysome analysis were done as described previously (Fristedt *et*  
580 *al.*, 2014) but using Hybond-N membranes (GE Healthcare Life Sciences). Probes were amplified  
581 from total plant DNA using gene-specific primers (Table S2), radioactively labeled using the  
582 Megaprime DNA Labeling System (GE Healthcare Life Sciences), and hybridized at 65 °C.

## 583 Thermotolerance tests

584 Arabidopsis seeds of WT, *cia2-2*, *cil-1*, and *cia2-2 cil-1* plants were surface sterilized by  
585 soaking in a 50% (v/v) commercial bleach solution for 7 min. The seeds were then rinsed five times  
586 with sterile water and resuspended in 1 ml of 0.1% (w/v) agarose solution. The seeds were stratified  
587 for 2 days at 4 °C. They were then placed evenly onto plates with 35 ml of ½ MS medium with agar  
588 at pH 5.8. Each plate was divided into four equal parts, one part per genotype, and approximately  
589 25 seeds of every genotype were sown on a single plate. The plates were parafilm sealed to prevent  
590 dehydration of growing plants. The seeds were germinated and cultivated for 7 days under standard  
591 growth conditions.

592 After 7 days of *in vitro* cultivation, the seedlings were subjected to thermotolerance assay  
593 according to a previously described procedure (Silva-Correia *et al.*, 2014). Heat treatment was  
594 performed under ambient laboratory light after 3 h of light photoperiod. Parafilm-sealed plates with  
595 grown seedlings were set in a water bath preheated to 45 °C for 20, 30, or 40 min. After the  
596 treatment, the plates were transferred again to the growth chamber where the plants were cultivated  
597 for subsequent 7 days.

598 The survival rate of seedlings of individual genotypes was evaluated from the heat-treated  
599 plants' ability to produce new green leaves 7 days after the treatment. The plants were imaged, and  
600 the proportion of seedlings survived after heat treatment and all germinated plants was calculated  
601 for each genotype at every timepoint.

## 602 Accession numbers

603 The following gene names are used in Figure 5: *Rps6* (AT1G64510), *Rpl11* (AT1G32990),  
604 *Rpl18* (AT1G48350), *Rpl28* (AT2G33450), *Rpl3* (AT2G43030), *Rpl21* (AT1G35680), *PSRP2*  
605 (*AT3G52150*), *Rpl9* (AT3G44890), *Rps17* (AT1G79850), *Rps5* (AT2G33800), *Rps10* (AT3G13120),  
606 *Rpl17* (AT3G54210), *Rpl13* (AT1G78630), *PSRP4* (AT2G38140), *Rps9* (AT1G74970), *Rps21*  
607 (*AT3G27160*), *rpl2* (ATCG01310 and ATCG00830), *Rps20* (AT3G15190), *Rpl19.1* (AT4G17560),  
608 *Rpl19.2* (AT5G47190), *Rpl29* (AT5G65220), *rpl32* (ATCG01020), *DG1* (AT5G67570), *PPR2*  
609 (*AT3G06430*), *SVR7* (AT4G16390), *PPR5* (AT4G39620), *EMB2279* (AT1G30610), *PDM1/SEL1*  
610 (*AT4G18520*) *PPR596* (AT1G80270), *HCF152* (AT3G09650), *PSRP1* (AT5G24490), *PBR1*



20

611 (*AT1G71720*), *IF3-4* (*AT4G30690*), *IF3-2* (*AT2G24060*), *cpHSC70-2* (*AT5G49910*), and *SVR3*  
612 (*AT5G13650*).

## 613 Acknowledgments

614 We thank Prof. Ralph Bock for *psrp5-R1* and *rps17-1* seeds and Prof. Dario Leister for  
615 *prpl11-1* and *prps1-1* seeds. We thank Dr. Peter Robert Kindgren for help with *PPR* gene analysis  
616 and Dr. Anna Kozłowska-Makulska for technical help during the cHL screening. P.G., P.B., J.M.,  
617 M.Z., and S.K. acknowledge financial support from the Polish National Science Center (Narodowe  
618 Centrum Nauki; OPUS6, UMO-2013/11/B/NZ3/00973 and MAESTRO6  
619 UMO-2014/14/A/NZ1/00218 given to S.K.). L.B.S. acknowledges financial support from the  
620 Independent Research Fund Denmark (Danmarks Frie Forskningsfond; 7014-00322B). C.W.  
621 acknowledges financial support from the Academy of Finland (Decision 294580).

## 622 Short legends for Supporting Information

623 **Table S1.** List of genes selected from targeted reverse genetic screen for subcellular  
624 localization experiments.

625 **Table S2.** List of primers used in this study.

626 **Figure S1.** Examples of results obtained from the initial reverse genetic screening in UV-AB  
627 and high-light experiments.

628 **Figure S2.** Subcellular localization of CIA2<sup>1-100</sup>:YFP and 100 aa N-terminal part of CIA2  
629 fused to yellow fluorescence protein (YFP) at C termini.

630 **Figure S3.** Isolation and characterization of *cia2-2 cil-2* double mutant.

631 **Figure S4.** High-light (HL) and UV-AB susceptibility of *cia2-2 cil-2*.

632 **Figure S5.** CIA2 and CIL are required for optimal photosynthesis in Arabidopsis.

633 **Figure S6.** Analysis of rRNA and NPQ in plastid translation mutants.

634 **Data S1.** List of T-DNA mutants used in targeted reverse genetic screen.

635 **Data S2.** List of genes differentially expressed in *cia2-2 cil-1* compared to Col-0.

## 636 Conflict of interest

637 No conflicts of interest.

## 638 Author contributions

639 P.G., C.W., and S.K. formulated the hypothesis and conceived the research plan. P.G., P.B.,  
640 L.B.S., M.Z., and J.M. performed the experiments; P.G., P.B., and L.B.S. analyzed the data; P.G.,



21

641 C.W., and S.K. supervised the analysis; and P.G., P.B., C.W., L.B.S., and S.K. wrote the article,  
642 with contributions from all authors.

## 643 References

- 644 **Barajas-López, J. de D., Blanco, N.E. and Strand, Å.** (2013) Plastid-to-nucleus communication,  
645 signals controlling the running of the plant cell. *Biochim. Biophys. Acta - Mol. Cell Res.*, **1833**,  
646 425–437.
- 647 **Barkan, A. and Small, I.** (2014) Pentatricopeptide Repeat Proteins in Plants. *Annu. Rev. Plant*  
648 *Biol.*, **65**, 415–442.
- 649 **Bernacki, M.J., Czarnocka, W., Szechyńska-Hebda, M., Mittler, R. and Karpiński, S.** (2019)  
650 Biotechnological Potential of LSD1, EDS1, and PAD4 in the Improvement of Crops and  
651 Industrial Plants. *Plants*, **8**, 290.
- 652 **Białasek, M., Górecka, M., Mittler, R. and Karpiński, S.** (2017) Evidence for the Involvement of  
653 Electrical, Calcium and ROS Signaling in the Systemic Regulation of Non-Photochemical  
654 Quenching and Photosynthesis. *Plant Cell Physiol.*, **58**, 207–215.
- 655 **Bieri, P., Leibundgut, M., Saurer, M., Boehringer, D. and Ban, N.** (2017) The complete  
656 structure of the chloroplast 70S ribosome in complex with translation factor pY. *EMBO J.*, **36**,  
657 475–486.
- 658 **Bollenbach, T.J., Lange, H., Gutierrez, R., Erhardt, M., Stern, D.B. and Gagliardi, D.** (2005)  
659 RNR1, a 3'-5' exoribonuclease belonging to the RNR superfamily, catalyzes 3' maturation of  
660 chloroplast ribosomal RNAs in *Arabidopsis thaliana*. *Nucleic Acids Res.*, **33**, 2751–2763.
- 661 **Bollenbach, T.J., Schuster, G., Portnoy, V. and Stern, D.B.** (2007) Processing, degradation, and  
662 polyadenylation of chloroplast transcripts. In *Topics in Current Genetics*. pp. 175–211.
- 663 **Burdiak, P., Rusaczek, A., Witoń, D., Główny, D. and Karpiński, S.** (2015) Cysteine-rich  
664 receptor-like kinase CRK5 as a regulator of growth, development, and ultraviolet radiation  
665 responses in *Arabidopsis thaliana*. *J. Exp. Bot.*, **66**, 3325–3337.
- 666 **Caldwell, C.R.** (1993) Ultraviolet-Induced Photodegradation of Cucumber (*Cucumis sativus* L.)  
667 Microsomal and Soluble Protein Tryptophanyl Residues in Vitro. *Plant Physiol.*, **101**, 947–  
668 953.
- 669 **Caplan, J.L., Kumar, A.S., Park, E., Padmanabhan, M.S., Hoban, K., Modla, S., Czymmek,**  
670 **K. and Dinesh-Kumar, S.P.** (2015) Chloroplast Stromules Function during Innate Immunity.  
671 *Dev. Cell*, **34**, 45–57.
- 672 **Casati, P. and Walbot, V.** (2004) Crosslinking of Ribosomal Proteins to RNA in Maize  
673 Ribosomes by UV-B and Its Effects on Translation. *Plant Physiol.*, **136**, 3319–3332.
- 674 **Chan, K.X., Mabbitt, P.D., Phua, S.Y., et al.** (2016) Sensing and signaling of oxidative stress in  
675 chloroplasts by inactivation of the SAL1 phosphoadenosine phosphatase. *Proc. Natl. Acad.*  
676 *Sci.*, **113**, E4567–E4576.



- 677 **Chi, W., Sun, X. and Zhang, L.** (2013) Intracellular Signaling from Plastid to Nucleus. *Annu. Rev.*  
678 *Plant Biol.*, **64**, 559–582.
- 679 **Chotewutmontri, P. and Barkan, A.** (2018) Multilevel effects of light on ribosome dynamics in  
680 chloroplasts program genome-wide and psbA-specific changes in translation T. Burch-Smith,  
681 ed. *PLOS Genet.*, **14**, e1007555.
- 682 **Clercq, I. De, Vermeirssen, V., Aken, O. Van, et al.** (2013) The membrane-bound NAC  
683 transcription factor ANAC013 functions in mitochondrial retrograde regulation of the  
684 oxidative stress response in Arabidopsis. *Plant Cell*, **25**, 3472–3490.
- 685 **Daniell, H., Lin, C.-S., Yu, M. and Chang, W.-J.** (2016) Chloroplast genomes: diversity,  
686 evolution, and applications in genetic engineering. *Genome Biol.*, **17**, 134.
- 687 **Dickinson, P.J., Kumar, M., Martinho, C., et al.** (2018) Chloroplast Signaling Gates  
688 Thermotolerance in Arabidopsis. *Cell Rep.*, **22**, 1657–1665.
- 689 **Distelbarth, H., Nägele, T. and Heyer, A.G.** (2013) Responses of antioxidant enzymes to cold and  
690 high light are not correlated to freezing tolerance in natural accessions of Arabidopsis thaliana  
691 F. Loreto, ed. *Plant Biol.*, **15**, 982–990.
- 692 **Dogra, V., Li, Mingyue, Singh, S., Li, Mengping and Kim, C.** (2019) Oxidative post-  
693 translational modification of EXECUTER1 is required for singlet oxygen sensing in plastids.  
694 *Nat. Commun.*, **10**, 2834.
- 695 **Eberhard, S., Drapier, D. and Wollman, F.A.** (2002) Searching limiting steps in the expression  
696 of chloroplast-encoded proteins: Relations between gene copy number, transcription, transcript  
697 abundance and translation rate in the chloroplast of Chlamydomonas reinhardtii. *Plant J.*, **31**,  
698 149–160.
- 699 **Estavillo, G.M., Chan, K.X., Phua, S.Y. and Pogson, B.J.** (2013) Reconsidering the nature and  
700 mode of action of metabolite retrograde signals from the chloroplast. *Front. Plant Sci.*, **3**, 1–9.
- 701 **Estavillo, G.M., Crisp, P. a., Pornsiriwong, W., et al.** (2011) Evidence for a SAL1-PAP  
702 Chloroplast Retrograde Pathway That Functions in Drought and High Light Signaling in  
703 Arabidopsis. *Plant Cell*, **23**, 3992–4012.
- 704 **Exposito-Rodriguez, M., Laissue, P.P., Yvon-Durocher, G., Smirnoff, N. and Mullineaux,**  
705 **P.M.** (2017) Photosynthesis-dependent H<sub>2</sub>O<sub>2</sub> transfer from chloroplasts to nuclei provides a  
706 high-light signalling mechanism. *Nat. Commun.*, **8**, 49.
- 707 **Ferreira, M.L.F., Pezza, A., Biarc, J., Burlingame, A.L. and Casati, P.** (2010) Plant L10  
708 ribosomal proteins have different roles during development and translation under ultraviolet-B  
709 stress. *Plant Physiol.*, **153**, 1878–1894.
- 710 **Finkelstein, R., Lynch, T., Reeves, W., Petitfils, M. and Mostachetti, M.** (2011) Accumulation  
711 of the transcription factor ABA-insensitive (ABI)4 is tightly regulated post-transcriptionally. *J.*  
712 *Exp. Bot.*, **62**, 3971–3979.



23

- 713 **Fristedt, R., Scharff, L.B., Clarke, C. a, Wang, Q., Lin, C., Merchant, S.S. and Bock, R. (2014)**  
714 RBF1, a plant homolog of the bacterial ribosome-binding factor RbfA, acts in processing of  
715 the chloroplast 16S ribosomal RNA. *Plant Physiol.*, **164**, 201–15.
- 716 **Gawronski, P., Witon, D., Vashutina, K., Bederska, M., Betlinski, B., Rusaczonek, A. and**  
717 **Karpinski, S. (2014)** Mitogen-activated protein kinase 4 is a salicylic acid-independent  
718 regulator of growth but not of photosynthesis in Arabidopsis. *Mol. Plant*, **7**, 1151–1166.
- 719 **Gilroy, S., Bialasek, M., Suzuki, N., Górecka, M., Devireddy, A.R., Karpiński, S. and Mittler,**  
720 **R. (2016)** ROS, Calcium, and Electric Signals: Key Mediators of Rapid Systemic Signaling in  
721 Plants. *Plant Physiol.*, **171**, 1606–1615.
- 722 **Grabowski, E., Miao, Y., Mulisch, M. and Krupinska, K. (2008)** Single-Stranded DNA-Binding  
723 Protein Whirly1 in Barley Leaves Is Located in Plastids and the Nucleus of the Same Cell.  
724 *Plant Physiol.*, **147**, 1800–1804.
- 725 **Guo, H., Feng, P., Chi, W., et al. (2016)** Plastid-nucleus communication involves calcium-  
726 modulated MAPK signalling. *Nat. Commun.*, **7**, 1–15.
- 727 **Gururani, M.A., Venkatesh, J. and Tran, L.S.P. (2015)** Regulation of photosynthesis during  
728 abiotic stress-induced photoinhibition. *Mol. Plant*, **8**, 1304–1320.
- 729 **Herdean, A., Teardo, E., Nilsson, A.K., et al. (2016)** A voltage-dependent chloride channel fine-  
730 tunes photosynthesis in plants. *Nat. Commun.*, **7**, 11654.
- 731 **Hollósy, F. (2002)** Effects of ultraviolet radiation on plant cells. *Micron*, **33**, 179–197.
- 732 **Jarvis, P. (2008)** Targeting of nucleus-encoded proteins to chloroplasts in plants. *New Phytol.*, **179**,  
733 257–285.
- 734 **Jarvis, P. and López-Juez, E. (2013)** Biogenesis and homeostasis of chloroplasts and other  
735 plastids. *Nat. Rev. Mol. Cell Biol.*, **14**, 787–802.
- 736 **Jarvis, P. and Robinson, C. (2004)** Mechanisms of protein import and routing in chloroplasts.  
737 *Curr. Biol.*, **14**, 1064–1077.
- 738 **Jaspers, P., Blomster, T., Brosché, M., et al. (2009)** Unequally redundant RCD1 and SRO1  
739 mediate stress and developmental responses and interact with transcription factors. *Plant J.*,  
740 **60**, 268–279.
- 741 **Jin, J., Zhang, H., Kong, L., Gao, G. and Luo, J. (2014)** PlantTFDB 3.0: A portal for the  
742 functional and evolutionary study of plant transcription factors. *Nucleic Acids Res.*, **42**, 1182–  
743 1187.
- 744 **Kacprzak, S.M., Mochizuki, N., Naranjo, B., Xu, D., Leister, D., Kleine, T., Okamoto, H. and**  
745 **Terry, M.J. (2019)** Plastid-to-Nucleus Retrograde Signalling during Chloroplast Biogenesis  
746 Does Not Require ABI4. *Plant Physiol.*, **179**, 18–23.
- 747 **Karpinski, S., Escobar, C., Karpinska, B., Creissen, G. and Mullineaux, P.M. (1997)**  
748 Photosynthetic electron transport regulates the expression of cytosolic ascorbate peroxidase  
749 genes in Arabidopsis during excess light stress. *Plant Cell*, **9**, 627–640.



24

- 750 **Karpiński, S., Reynolds, H., Karpinska, B., Wingsle, G., Creissen, G. and Mullineaux, P.M.**  
751 (1999) Systemic Signaling and Acclimation in Response to Excess Excitation Energy in  
752 Arabidopsis. *Science*, **284**, 654–657.
- 753 **Krause, K., Oetke, S. and Krupinska, K.** (2012) Dual Targeting and Retrograde Translocation:  
754 Regulators of Plant Nuclear Gene Expression Can Be Sequestered by Plastids. *Int. J. Mol. Sci.*,  
755 **13**, 11085–11101.
- 756 **Kulasek, M., Bernacki, M.J., Ciszak, K., Witoń, D. and Karpiński, S.** (2016) Contribution of  
757 PsbS function and stomatal conductance to foliar temperature in higher plants. *Plant Cell*  
758 *Physiol.*, **57**, 1495–1509.
- 759 **Lee, K.P., Kim, C., Landgraf, F. and Apel, K.** (2007) EXECUTER1- and EXECUTER2-  
760 dependent transfer of stress-related signals from the plastid to the nucleus of Arabidopsis  
761 thaliana. *Proc Natl Acad Sci U S A*, **104**, 10270–10275.
- 762 **Leister, D. and Kleine, T.** (2008) Towards a comprehensive catalog of chloroplast proteins and  
763 their interactions. *Cell Res.*, **18**, 1081–1083.
- 764 **Li, J.F., Park, E., Arnim, A.G. Von and Nebenführ, A.** (2009) The FAST technique: A  
765 simplified Agrobacterium-based transformation method for transient gene expression analysis  
766 in seedlings of Arabidopsis and other plant species. *Plant Methods*, **5**, 1–15.
- 767 **Li, M., Hensel, G., Mascher, M., et al.** (2019) Leaf Variegation and Impaired Chloroplast  
768 Development Caused by a Truncated CCT Domain Gene in alboblasts Barley. *Plant Cell*, **31**,  
769 1430–1445.
- 770 **Li, Z., Wakao, S., Fischer, B.B. and Niyogi, K.K.** (2009) Sensing and Responding to Excess  
771 Light. *Annu. Rev. Plant Biol.*, **60**, 239–260.
- 772 **Liere, K. and Börner, T.** (2007) Transcription and transcriptional regulation in plastids. In *Systems*  
773 *Biology*. pp. 121–174.
- 774 **Love, M.I., Huber, W. and Anders, S.** (2014) Moderated estimation of fold change and dispersion  
775 for RNA-seq data with DESeq2. *Genome Biol.*, **15**, 550.
- 776 **Mateo, A., Mühlenbock, P., Rustérucci, C., Chang, C.C., Misalski, Z., Karpinska, B., Parker,**  
777 **J.E., Mullineaux, P.M. and Karpinski, S.** (2004) LESION SIMULATING DISEASE 1 Is  
778 Required for Acclimation to Conditions That Promote Excess Excitation Energy. *Plant*  
779 *Physiol.*, **136**, 2818–2830.
- 780 **Miyata, K., Ikeda, H., Nakaji, M., Kanel, D.R. and Terashima, I.** (2015) Rate Constants of PSII  
781 Photoinhibition and its Repair, and PSII Fluorescence Parameters in Field Plants in Relation to  
782 their Growth Light Environments. *Plant Cell Physiol.*, **56**, 1841–1854.
- 783 **Mühlenbock, P., Szechynska-Hebda, M., Plaszczyca, M., Baudou, M., Mullineaux, P.M.,**  
784 **Parker, J.E., Karpinska, B. and Karpiński, S.** (2008) Chloroplast Signaling and LESION  
785 SIMULATING DISEASE1 Regulate Crosstalk between Light Acclimation and Immunity in  
786 Arabidopsis. *Plant Cell*, **20**, 2339–2356.



25

- 787 **Mullineaux, P.M., Karpiński, S. and Baker, N.R.** (2006) Spatial Dependence for Hydrogen  
788 Peroxide-Directed Signaling in Light-Stressed Plants. *Plant Physiol.*, **141**, 346–350.
- 789 **Myouga, F., Akiyama, K., Tomonaga, Y., Kato, A., Sato, Y., Kobayashi, M., Nagata, N.,**  
790 **Sakurai, T. and Shinozaki, K.** (2013) The chloroplast function database II: A comprehensive  
791 collection of homozygous mutants and their phenotypic/genotypic traits for nuclear-encoded  
792 chloroplast proteins. *Plant Cell Physiol.*, **54**, 1–10.
- 793 **Nakagawa, T., Kurose, T., Hino, T., et al.** (2007) Development of series of gateway binary  
794 vectors, pGWBs, for realizing efficient construction of fusion genes for plant transformation.  
795 *J. Biosci. Bioeng.*, **104**, 34–41.
- 796 **Nakai, M.** (2015) The TIC complex uncovered: The alternative view on the molecular mechanism  
797 of protein translocation across the inner envelope membrane of chloroplasts. *Biochim.*  
798 *Biophys. Acta - Bioenerg.*, **1847**, 957–967.
- 799 **Ng, S., Ivanova, A., Duncan, O., et al.** (2013) A Membrane-Bound NAC Transcription Factor,  
800 ANAC017, Mediates Mitochondrial Retrograde Signaling in Arabidopsis. *Plant Cell*, **25**,  
801 3450–3471.
- 802 **Nickelsen, J., Bohne, A.-V. and Westhoff, P.** (2014) Chloroplast Gene Expression—Translation.  
803 In *Plastid Biology*. New York, NY: Springer New York, pp. 49–78.
- 804 **Nishimura, K., Ashida, H., Ogawa, T. and Yokota, A.** (2010) A DEAD box protein is required  
805 for formation of a hidden break in Arabidopsis chloroplast 23S rRNA. *Plant J.*, **63**, 766–777.
- 806 **Niyogi, K.K., Li, X.P., Rosenberg, V. and Jung, H.S.** (2005) Is PsbS the site of non-  
807 photochemical quenching in photosynthesis? *J. Exp. Bot.*, **56**, 375–382.
- 808 **Nørholm, M.H.** (2010) A mutant Pfu DNA polymerase designed for advanced uracil-excision  
809 DNA engineering. *BMC Biotechnol.*, **10**, 21.
- 810 **Nour-Eldin, H.H., Hansen, B.G., Nørholm, M.H.H., Jensen, J.K. and Halkier, B.A.** (2006)  
811 Advancing uracil-excision based cloning towards an ideal technique for cloning PCR  
812 fragments. *Nucleic Acids Res.*, **34**, e122–e122.
- 813 **Page, M.T., Kacprzak, S.M., Mochizuki, N., Okamoto, H., Smith, A.G. and Terry, M.J.** (2017)  
814 Seedlings Lacking the PTM Protein Do Not Show a *genomes uncoupled (gun)* Mutant  
815 Phenotype. *Plant Physiol.*, **174**, 21–26.
- 816 **Paila, Y.D., Richardson, L.G.L. and Schnell, D.J.** (2015) New Insights into the Mechanism of  
817 Chloroplast Protein Import and Its Integration with Protein Quality Control, Organelle  
818 Biogenesis and Development. *J. Mol. Biol.*, **427**, 1038–1060.
- 819 **Parker, N., Wang, Y. and Meinke, D.** (2014) Natural Variation in Sensitivity to a Loss of  
820 Chloroplast Translation in Arabidopsis. *Plant Physiol.*, **166**, 2013–2027.
- 821 **Patro, R., Duggal, G., Love, M.I., Irizarry, R.A. and Kingsford, C.** (2017) Salmon provides fast  
822 and bias-aware quantification of transcript expression. *Nat. Methods*, **14**, 417–419.



- 823 **Pérez-Rodríguez, P., Riaño-Pachón, D.M., Corrêa, L.G.G., Rensing, S.A., Kersten, B. and**  
824 **Mueller-Roeber, B.** (2009) PlnTFDB: Updated content and new features of the plant  
825 transcription factor database. *Nucleic Acids Res.*, **38**, 822–827.
- 826 **Pesaresi, P., Masiero, S., Eubel, H., Braun, H.-P., Bhushan, S., Glaser, E., Salamini, F. and**  
827 **Leister, D.** (2006) Nuclear photosynthetic gene expression is synergistically modulated by  
828 rates of protein synthesis in chloroplasts and mitochondria. *Plant Cell*, **18**, 970–991.
- 829 **Pesaresi, P., Varotto, C., Meurer, J., Jahns, P., Salamini, F. and Leister, D.** (2001) Knock-out  
830 of the plastid ribosomal protein L11 in Arabidopsis: Effects on mRNA translation and  
831 photosynthesis. *Plant J.*, **27**, 179–189.
- 832 **Pogson, B.J., Woo, N.S., Förster, B. and Small, I.D.** (2008) Plastid signalling to the nucleus and  
833 beyond. *Trends Plant Sci*, **13**, 602–9.
- 834 **Ramakers, C., Ruijter, J.M., Deprez, R.H.L. and Moorman, A.F..** (2003) Assumption-free  
835 analysis of quantitative real-time polymerase chain reaction (PCR) data. *Neurosci Lett*, **339**,  
836 62–66.
- 837 **Ramel, F., Birtic, S., Ginies, C., Soubigou-Taconnat, L., Triantaphylides, C. and Havaux, M.**  
838 (2012) Carotenoid oxidation products are stress signals that mediate gene responses to singlet  
839 oxygen in plants. *Proc. Natl. Acad. Sci.*, **109**, 5535–5540.
- 840 **Romani, I., Tadini, L., Rossi, F., Masiero, S., Pribil, M., Jahns, P., Kater, M., Leister, D. and**  
841 **Pesaresi, P.** (2012) Versatile roles of Arabidopsis plastid ribosomal proteins in plant growth  
842 and development. *Plant J.*, **72**, 922–934.
- 843 **Scharff, L.B. and Bock, R.** (2014) Synthetic biology in plastids. *Plant J.*, **78**, 783–798.
- 844 **Schreiber, U. and Klughammer, C.** (2008) New accessory for the DUAL-PAM-100: The  
845 P515/535 module and examples of its application. *PAM Appl. Notes*, **1**, 1–10.
- 846 **Schwacke, R., Schneider, A., Graaff, E. Van Der, Fischer, K., Catoni, E., Desimone, M.,**  
847 **Frommer, W.B., Flügge, U.I. and Kunze, R.** (2003) ARAMEMNON, a novel database for  
848 Arabidopsis integral membrane proteins. *Plant Physiol.*, **131**, 16–26.
- 849 **Shapiguzov, A., Vainonen, J.P., Hunter, K., et al.** (2019) Arabidopsis RCD1 coordinates  
850 chloroplast and mitochondrial functions through interaction with ANAC transcription factors.  
851 *Elife*, **8**, 1–35.
- 852 **Silva-Correia, J., Freitas, S., Tavares, R.M., Lino-Neto, T. and Azevedo, H.** (2014) Phenotypic  
853 analysis of the Arabidopsis heat stress response during germination and early seedling  
854 development. *Plant Methods*, **10**, 7.
- 855 **Silvestro, D., Andersen, T.G., Schaller, H. and Jensen, P.E.** (2013) Plant Sterol Metabolism.  $\Delta 7$ -  
856 Sterol-C5-Desaturase (STE1/DWARF7),  $\Delta 5,7$ -Sterol- $\Delta 7$ -Reductase (DWARF5) and  $\Delta 24$ -  
857 Sterol- $\Delta 24$ -Reductase (DIMINUTO/DWARF1) Show Multiple Subcellular Localizations in  
858 Arabidopsis thaliana (Heynh) L J. L. Heazlewood, ed. *PLoS One*, **8**, e56429.
- 859 **Smirnov, N. and Arnaud, D.** (2019) Hydrogen peroxide metabolism and functions in plants. *New*  
860 *Phytol.*, **221**, 1197–1214.



- 861 **Soneson, C., Love, M.I. and Robinson, M.D.** (2016) Differential analyses for RNA-seq:  
862 transcript-level estimates improve gene-level inferences. *F1000Research*, **4**, 1521.
- 863 **Souza, A. de, Wang, J.-Z. and Dehesh, K.** (2017) Retrograde Signals: Integrators of  
864 Interorganellar Communication and Orchestrators of Plant Development. *Annu. Rev. Plant*  
865 *Biol.*, **68**, 85–108.
- 866 **Strayer, C., Oyama, T., Schultz, T., Raman, R., Somers, D., Mas, P., Panda, S., Kreps, J. and**  
867 **Kay, S.** (2000) Cloning of the Arabidopsis Clock Gene TOC1, an Autoregulatory Response  
868 Regulator Homolog. *Science (80-. )*, **289**, 768–771.
- 869 **Sugiura, M.** (2014) Plastid mRNA Translation. In *Chloroplast Biotechnology*. pp. 73–91.
- 870 **Sumanta, N., Haque, C., Nishika, J. and Suprakash, R.** (2014) Spectrophotometric Analysis of  
871 Chlorophylls and Carotenoids from Commonly Grown Fern Species by Using Various  
872 Extracting Solvents. *Res. J. Chem. Sci.*, **4**, 2231–606.
- 873 **Sun, C.-W., Chen, L.-J., Lin, L.-C. and Li, H.** (2001) Leaf-Specific Upregulation of Chloroplast  
874 Translocon Genes by a CCT Motif-Containing Protein, CIA2. *Plant Cell*, **13**, 2053–2061.
- 875 **Sun, C.-W., Huang, Y.-C. and Chang, H.-Y.** (2009) CIA2 Coordinately Up-Regulates Protein  
876 Import and Synthesis in Leaf Chloroplasts. *Plant Physiol.*, **150**, 879–888.
- 877 **Sun, Q., Zybaïlov, B., Majeran, W., Friso, G., Olinares, P.D.B. and Wijk, K.J. van** (2009)  
878 PPDB, the Plant Proteomics Database at Cornell. *Nucleic Acids Res.*, **37**, D969–D974.
- 879 **Tadini, L., Pesaresi, P., Kleine, T., et al.** (2016) GUN1 Controls Accumulation of the Plastid  
880 Ribosomal Protein S1 at the Protein Level and Interacts with Proteins Involved in Plastid  
881 Protein Homeostasis. *Plant Physiol.*, **170**, 1817–30.
- 882 **Tiller, N., Weingartner, M., Thiele, W., Maximova, E., Sch??ttler, M.A. and Bock, R.** (2012)  
883 The plastid-specific ribosomal proteins of Arabidopsis thaliana can be divided into non-  
884 essential proteins and genuine ribosomal proteins. *Plant J.*, **69**, 302–316.
- 885 **Wagner, R. and Pfannschmidt, T.** (2006) Eukaryotic transcription factors in plastids -  
886 Bioinformatic assessment and implications for the evolution of gene expression machineries in  
887 plants. *Gene*, **381**, 62–70.
- 888 **Wang, L., Kim, C., Xu, X., Piskurewicz, U., Dogra, V. and Singh, S.** (2016) Singlet oxygen- and  
889 EXECUTER1-mediated signaling is initiated in grana margins and depends on the. *Proc Natl*  
890 *Acad Sci U S A*, **113**, E3792–E3800.
- 891 **Waters, M.T., Wang, P., Korkaric, M., Capper, R.G., Saunders, N.J. and Langdale, J. a**  
892 (2009) GLK transcription factors coordinate expression of the photosynthetic apparatus in  
893 Arabidopsis. *Plant Cell*, **21**, 1109–1128.
- 894 **Wituszyńska, W., Ślesak, I., Vanderauwera, S., et al.** (2013) LESION SIMULATING  
895 DISEASE1, ENHANCED DISEASE SUSCEPTIBILITY1, and PHYTOALEXIN  
896 DEFICIENT4 Conditionally Regulate Cellular Signaling Homeostasis, Photosynthesis, Water  
897 Use Efficiency, and Seed Yield in Arabidopsis. *Plant Physiol.*, **161**, 1795–1805.



28

- 898 **Wituszyńska, W., Szechyńska-Hebda, M., Sobczak, M., Rusaczonek, A., Kozłowska-**  
899 **Makulska, A., Witoń, D. and Karpiński, S. (2015) LESION SIMULATING DISEASE 1**  
900 **And ENHANCED DISEASE SUSCEPTIBILITY 1 differentially regulate UV-C-induced**  
901 **photooxidative stress signalling and programmed cell death in Arabidopsis thaliana. *Plant,***  
902 ***Cell Environ.*, **38**, 315–330.**
- 903 **Wu, G.-Z., Chalvin, C., Hoelscher, M.P., Meyer, E.H., Wu, X.N. and Bock, R. (2018) Control**  
904 **of Retrograde Signaling by Rapid Turnover of GENOMES UNCOUPLED 1. *Plant Physiol.*,**  
905 ****176**, pp.00009.2018.**
- 906 **Wu, G., Meyer, E.H., Richter, A.S., et al. (2019) Control of retrograde signalling by protein**  
907 **import and cytosolic folding stress. *Nat. Plants*, **5**, 525–538.**
- 908 **Yabuta, Y., Motoki, T., Yoshimura, K., Takeda, T., Ishikawa, T. and Shigeoka, S. (2002)**  
909 **Thylakoid membrane-bound ascorbate peroxidase is a limiting factor of antioxidative systems**  
910 **under photo-oxidative stress. *Plant J.*, **32**, 915–925.**
- 911 **Yasumura, Y., Moylan, E.C. and Langdale, J.A. (2005) A Conserved Transcription Factor**  
912 **Mediates Nuclear Control of Organelle Biogenesis in Anciently Diverged Land Plants. *Plant***  
913 ***Cell*, **17**, 1894–1907.**
- 914 **Zoschke, R. and Bock, R. (2018) Chloroplast Translation: Structural and Functional Organization,**  
915 **Operational Control and Regulation. *Plant Cell*, **30**, tpc.00016.2018.**



# Figure legends

**Figure 1.** Isolation and characterization of *cia2-2 cil-1* double mutant. **(a, b)** Isolation of *cia2-4* mutant in reverse genetic screening using UV-AB **(a)** and high light in combination with low temperature (cHL) **(b)**. **(c)** In the upper part, a schematic representation of *CIA2* and *CIL* genes is presented. Black and white rectangles represent exons and untranslated regions, respectively. The lower part shows the analysis of functional domains in *CIA2* and *CIL* proteins: cTP–chloroplast transit peptide, NLS–nuclear localization signal, CCT–putative active domain in *CIA2* and *CIL*. The CCT domain contains NLS; however, it is not shown in the diagram for simplicity. **(d)** Phenotypes of 4-week-old plants grown in long-day conditions. *cia2-2* and *cia2-2 cil-1* plants were paler than the rest of analyzed genotypes; thus, the content of photosynthetic pigments was measured and shown in **(e)**. **(f)** Expression of *CIA2* and *CIL* in the analyzed genotypes was measured using qRT-PCR with gene-specific primers. Locations of primers are depicted in panel **(a)**. **(g, h)** Complementation of *cia2-2* phenotype with ectopic expression of *CIA2* under 35S and native promoter. **(g)** Relative expression of *CIA2* in analyzed lines. **(h)** Relative content of photosynthetic pigments in complementation lines. In **(a)**, **(e)** and **(f)** statistical significance (ANOVA and Tukey HSD test) is shown relative to Col-0 (\*\* $p < 0.01$ ; \*\*\* $p < 0.001$ ). In **(g)** and **(h)** statistical significance (ANOVA and Tukey HSD test) is shown relative to *cia2-2* (\*\* $p < 0.01$ ; \*\*\* $p < 0.001$ ) and to Col-0 ( $^{\wedge}p < 0.05$ ;  $^{\wedge\wedge}p < 0.01$ ;  $^{\wedge\wedge\wedge}p < 0.001$ ).

**Figure 2.** *CIA2* and *CIL* are required for resistance to UV-AB. Mature plants were exposed to UV-AB, and the plants' performance was assessed using chlorophyll *a* fluorescence **(a and b)** and ion leakage **(c)**. **(a)** Maximum efficiency of PSII ( $F_v/F_m$ ), nonregulated energy dissipation ( $Y(NO)$ ), and nonphotochemical quenching (NPQ) were measured before and after UV-AB treatment (1 and 2 days). Each point represents mean  $\pm$ SEM of at least eight plants. **(b)**  $F_v/F_m$  of control (UV-) and UV-AB-treated (UV +) plants of Col-0 and *cia2-2 cil-1* plants. Values of  $F_v/F_m$  are shown in pseudocolor scale. **(c)** Ion leakage of control (UV-,  $n = 5$ ) and UV-AB-treated (UV +,  $n = 18$ ) plants is shown as a percentage of total ion leakage. Statistical significance (ANOVA and Tukey HSD test) is shown relative to Col-0 (\* $p < 0.05$ ; \*\*\* $p < 0.001$ ) and to control conditions ( $^{\wedge\wedge\wedge}p < 0.001$ ).

**Figure 3.** High-light (HL) susceptibility of *cia2-2 cil-1*. **(a)** Representation of Arabidopsis rosette with the young leaves marked with blue, dashed line. **(b, c, d)** Maximum efficiency of PSII ( $F_v/F_m$ ) measured in plants **(b)** exposed to blue HL ( $1100 \mu\text{mol m}^{-2} \text{s}^{-1}$ ) for a specific time ( $n = 4-8$  plants), **(c)** during recovery after HL stress,  $n = 6-8$ , **(d)** and treated with inhibitors influencing the production of ROS in chloroplasts ( $n = 12-22$ ). In each plot, points represent mean  $\pm$ SEM measured in independent plants **(b and c)** or leaf disks **(d)**. Statistical significance (ANOVA and Tukey HSD test) is shown relative to Col-0 (\* $p < 0.05$ ; \*\* $p < 0.01$ ; \*\*\* $p < 0.001$ )



30

950 **Figure 4.** CIA2 and CIL are required for optimal photosynthesis in Arabidopsis. (a)  
951 Nonphotochemical quenching (NPQ) in analyzed genotypes. Points represent mean  $\pm$ SEM of the  
952 whole rosette and only young leaves. (b) NPQ of Col-0 and *cia2-2 cil-1*. (c) Analysis of  
953 electrochromic pigment shift (ECS, P515) at 160 and 660  $\mu\text{mol m}^{-2} \text{s}^{-1}$  of actinic light. For  
954 simplicity, only Col-0 and *cia2-2 cil-1* are shown. ST—single turnover flash. Total ECS (ECS<sub>T</sub>) (d)  
955 and  $\Delta\text{pH}$  (e) in analyzed genotypes at 160 and 660  $\mu\text{mol m}^{-2} \text{s}^{-1}$ . Box plots represent values of 10  
956 independent plants. (f) CO<sub>2</sub> assimilation as a function of light intensity. (g) CO<sub>2</sub> assimilation as a  
957 function of CO<sub>2</sub> concentration. In (f) and (g), values represent mean  $\pm$ SEM of 7–9 plants. Statistical  
958 significance (ANOVA and Tukey HSD test) is shown relative to Col-0 (\* $p < 0.05$ ; \*\* $p < 0.01$ ;  
959 \*\*\* $p < 0.001$ )

960 **Figure 5.** Characterization of chloroplast translation in analyzed genotypes. (a) Expression analysis  
961 of genes encoding chloroplast ribosomal proteins. Levels of analyzed transcripts were determined  
962 using qRT-PCR and normalized to two house-keeping genes (*PP2AA3* and *TIP41L*). Bars indicate  
963 mean values  $\pm$ SD (three independent biological replicates). (b) Expression profile (RNA-seq) of  
964 genes involved in the regulation of plastid translation. (c) Polysome analysis reveals slower  
965 translation of *psbD* mRNA in *cia2-2 cil-1* double mutant as compared to Col-0. Gray triangles  
966 indicate the density of sucrose gradient. Methylene blue-stained 18S rRNA is shown as a loading  
967 control. (d) Susceptibility to chloroplast translation inhibitor (spectinomycin, 1.25 mg/L) of  
968 analyzed genotypes. Statistical significance (ANOVA and Tukey HSD test) is shown relative to  
969 Col-0 (\* $p < 0.05$ ; \*\* $p < 0.01$ ; \*\*\* $p < 0.001$ ).

970 **Figure 6.** Maturation of plastid rRNAs. (a) Plastid rRNA operon. Mature forms of 16 and 23S  
971 rRNA are shown. Precursor of 23S rRNA is processed and cleaved into three parts: 0.4, 1.1, and 1.3  
972 kb. (b) Relative abundance of precursor 23S and 16S rRNAs was measured using capillary  
973 electrophoresis and normalized to the cytoplasmic 18S rRNA. Values represent mean values  $\pm$  SEM  
974 ( $n = 3$ ). (c) Maturation and abundance of plastid rRNA were measured using Northern blot  
975 indicating that the 2.4 kb form of 23S rRNA is accumulated in *cia2-2 cil-1*. (d) Determination of  
976 relative amounts of 23S rRNA forms with qRT-PCR and primers (depicted in panel (a)) specific to  
977 each of cleaved fragments (primers A, B, and C) and flanking “hidden breaks” (primers AB and  
978 BC). Values were normalized to the level of 16S rRNA and represent mean values  $\pm$  SD ( $n = 3$ ).  
979 Statistical significance (ANOVA and Tukey HSD test) is shown relative to Col-0 (\* $p < 0.05$ ; \*\* $p <$   
980 0.01; \*\*\* $p < 0.001$ ).



31

981 **Figure 7.** CIA2 and CIL negatively regulate tolerance to heat shock. **(a)** Gene ontology (GO)  
 982 analysis of genes significantly induced in *cia2-2 cil-1* compared to Col-0 in the RNA-seq  
 983 experiment. Ten most significantly overrepresented GO terms are shown. Number of genes in each  
 984 group is shown in color of the bar. **(b)** Validation of expression of heat shock marker genes using  
 985 qRT-PCR in analyzed genotypes and additional allele (*cia2-3*) in Ler-0 background (n = 3). Error  
 986 bars represent  $\pm$  SD. **(c and d)** Thermo tolerance was tested in seedlings grown *in vitro*. Plants were  
 987 exposed to 45 °C for a specific period of time. **(c)** Pictures of plants grown in control conditions 7  
 988 days after heat shock. **(d)** Survival rate of control and heat shock-treated plants. Error bars represent  
 989  $\pm$ SEM (n  $\geq$  3 plates) from two independent experiments (in total at least 75 seedlings were analyzed  
 990 per genotype and treatment). Statistical significance (ANOVA and Tukey HSD test) is shown  
 991 relative to corresponding WT (\*\*\*)  $p < 0.001$ .

992



32

## 993 **Figures**



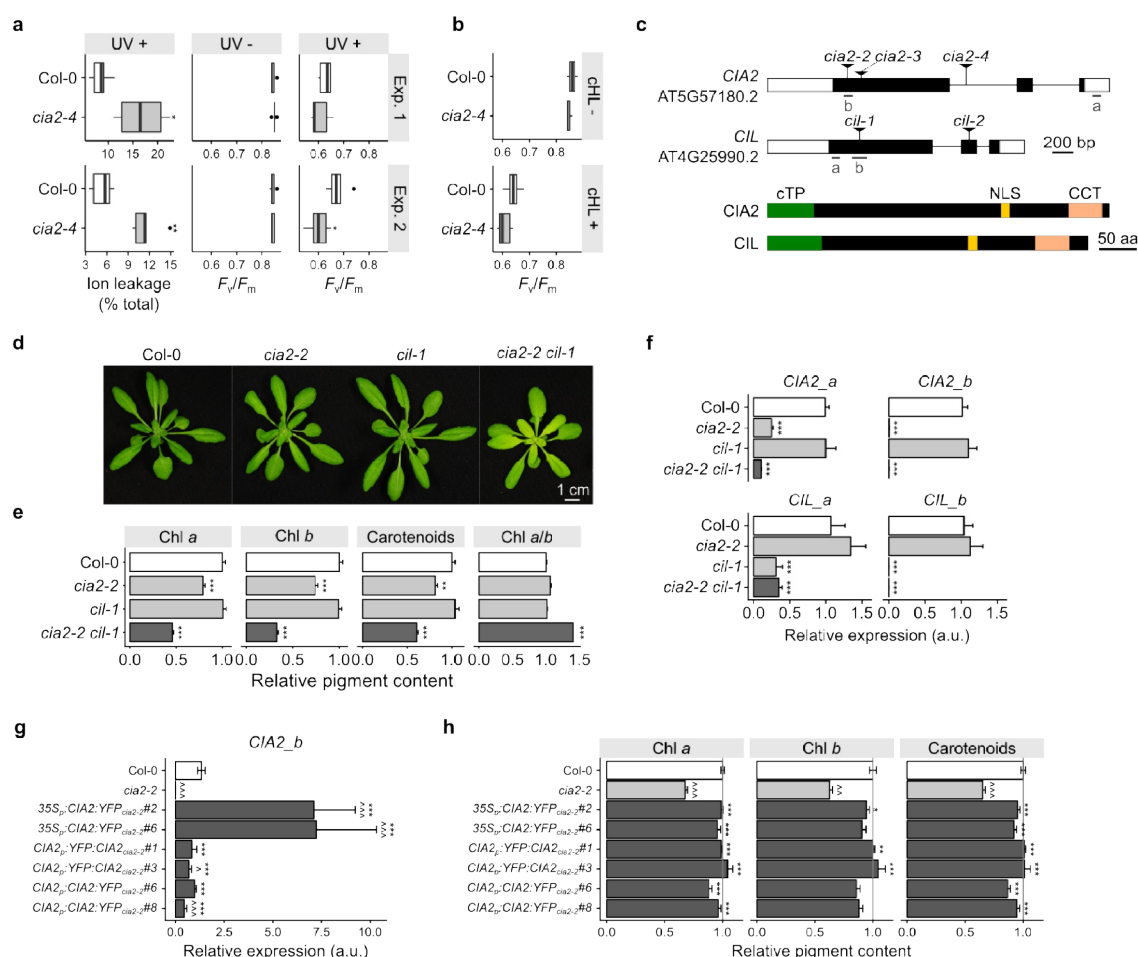


**Figure 1.** Isolation and characterization of *cia2-2 cil-1* double mutant. **(a, b)** Isolation of *cia2-4* mutant in reverse genetic screening using UV-AB **(a)** and high light in combination with low temperature (cHL) **(b)**. **(c)** In the upper part, a schematic representation of *CIA2* and *CIL* genes is presented. Black and white rectangles represent exons and untranslated regions, respectively. The lower part shows the analysis of functional domains in *CIA2* and *CIL* proteins: cTP—chloroplast transit peptide, NLS—nuclear localization signal, CCT—putative active domain in *CIA2* and *CIL*. The CCT domain contains NLS; however, it is not shown in the diagram for simplicity. **(d)** Phenotypes of 4-week-old plants grown in long-day conditions. *cia2-2* and *cia2-2 cil-1* plants were paler than the rest of analyzed genotypes; thus, the content of photosynthetic pigments was measured and shown in **(e)**. **(f)** Expression of *CIA2* and *CIL* in the analyzed genotypes was measured using qRT-PCR with gene-specific primers. Locations of primers are depicted in panel **(a)**. **(g, h)** Complementation of *cia2-2* phenotype with ectopic expression of *CIA2* under 35S and native promoter. **(g)** Relative expression of *CIA2* in analyzed lines. **(h)** Relative content of photosynthetic pigments in complementation lines. In **(a)**, **(e)** and **(f)** statistical significance (ANOVA and Tukey HSD test) is shown relative to Col-0 (\*\* $p < 0.01$ ; \*\*\* $p < 0.001$ ). In **(g)** and **(h)** statistical significance (ANOVA and Tukey HSD test) is shown relative to *cia2-2* (\*\* $p < 0.01$ ; \*\*\* $p < 0.001$ ) and to Col-0 ( $^{\wedge}p < 0.05$ ;  $^{\wedge\wedge}p < 0.01$ ;  $^{\wedge\wedge\wedge}p < 0.001$ ).



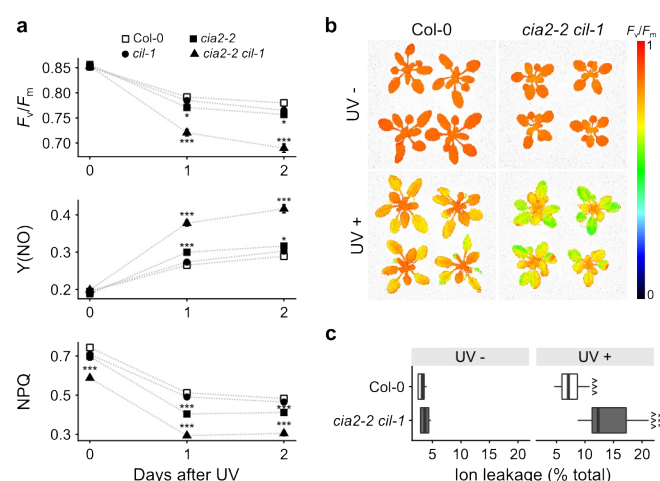


**Figure 2.** CIA2 and CIL are required for resistance to UV-AB. Mature plants were exposed to UV-AB, and the plants' performance was assessed using chlorophyll *a* fluorescence (**a** and **b**) and ion leakage (**c**). (**a**) Maximum efficiency of PSII ( $F_v/F_m$ ), nonregulated energy dissipation (Y(NO)), and nonphotochemical quenching (NPQ) were measured before and after UV-AB treatment (1 and 2 days). Each point represents mean  $\pm$ SEM of at least eight plants. (**b**)  $F_v/F_m$  of control (UV-) and UV-AB-treated (UV +) plants of Col-0 and *cia2-2 cil-1* plants. Values of  $F_v/F_m$  are shown in pseudocolor scale. (**c**) Ion leakage of control (UV-, n = 5) and UV-AB-treated (UV +, n = 18) plants is shown as a percentage of total ion leakage. Statistical significance (ANOVA and Tukey HSD test) is shown relative to Col-0 (\* $p < 0.05$ ; \*\*\* $p < 0.001$ ) and to control conditions (^^^ $p < 0.001$ ).



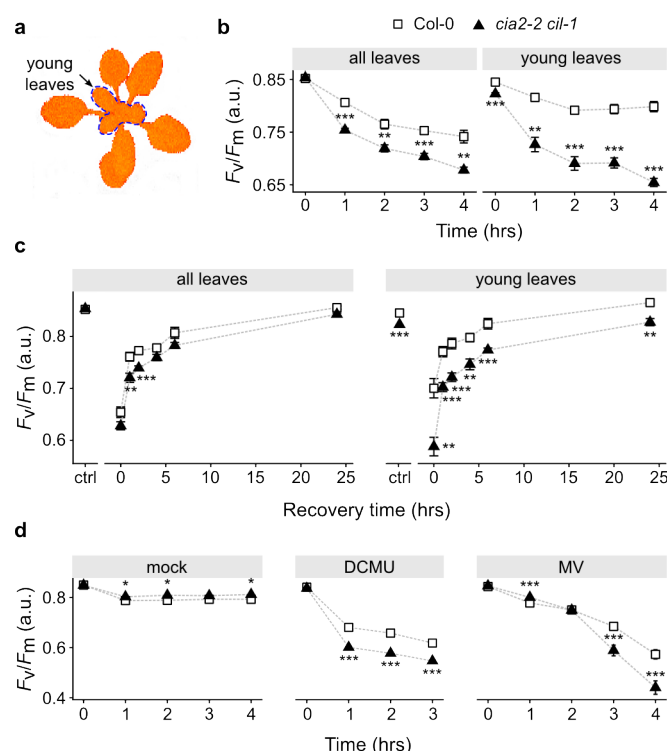


**Figure 3.** High-light (HL) susceptibility of *cia2-2 cil-1*. (a) Representation of Arabidopsis rosette with the young leaves marked with blue, dashed line. (b, c, d) Maximum efficiency of PSII ( $F_v/F_m$ ) measured in plants (b) exposed to blue HL ( $1100 \mu\text{mol m}^{-2} \text{s}^{-1}$ ) for a specific time ( $n = 4-8$  plants), (c) during recovery after HL stress,  $n = 6-8$ , (d) and treated with inhibitors influencing the production of ROS in chloroplasts ( $n = 12-22$ ). In each plot, points represent mean  $\pm$  SEM measured in independent plants (b and c) or leaf disks (d). Statistical significance (ANOVA and Tukey HSD test) is shown relative to Col-0 (\* $p < 0.05$ ; \*\*  $p < 0.01$ ; \*\*\* $p < 0.001$ )



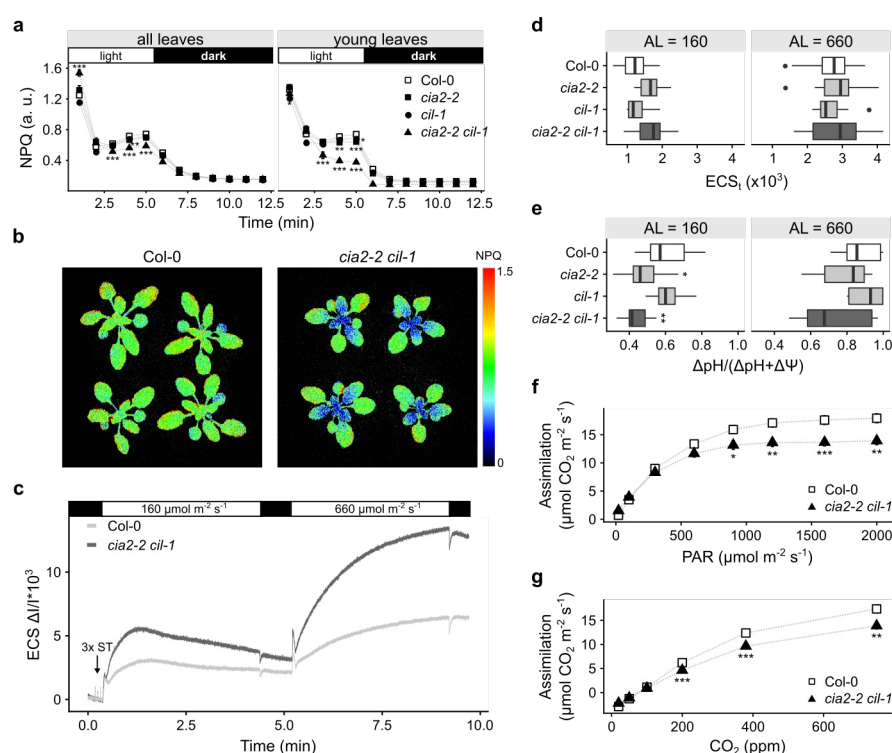


**Figure 4.** CIA2 and CIL are required for optimal photosynthesis in Arabidopsis. (a) Nonphotochemical quenching (NPQ) in analyzed genotypes. Points represent mean  $\pm$ SEM of the whole rosette and only young leaves. (b) NPQ of Col-0 and *cia2-2 cil-1*. (c) Analysis of electrochromic pigment shift (ECS, P515) at 160 and 660  $\mu\text{mol m}^{-2} \text{s}^{-1}$  of actinic light. For simplicity, only Col-0 and *cia2-2 cil-1* are shown. ST—single turnover flash. Total ECS (ECS<sub>t</sub>) (d) and  $\Delta\text{pH}$  (e) in analyzed genotypes at 160 and 660  $\mu\text{mol m}^{-2} \text{s}^{-1}$ . Box plots represent values of 10 independent plants. (f) CO<sub>2</sub> assimilation as a function of light intensity. (g) CO<sub>2</sub> assimilation as a function of CO<sub>2</sub> concentration. In (f) and (g), values represent mean  $\pm$ SEM of 7–9 plants. Statistical significance (ANOVA and Tukey HSD test) is shown relative to Col-0 (\* $p < 0.05$ ; \*\* $p < 0.01$ ; \*\*\* $p < 0.001$ )



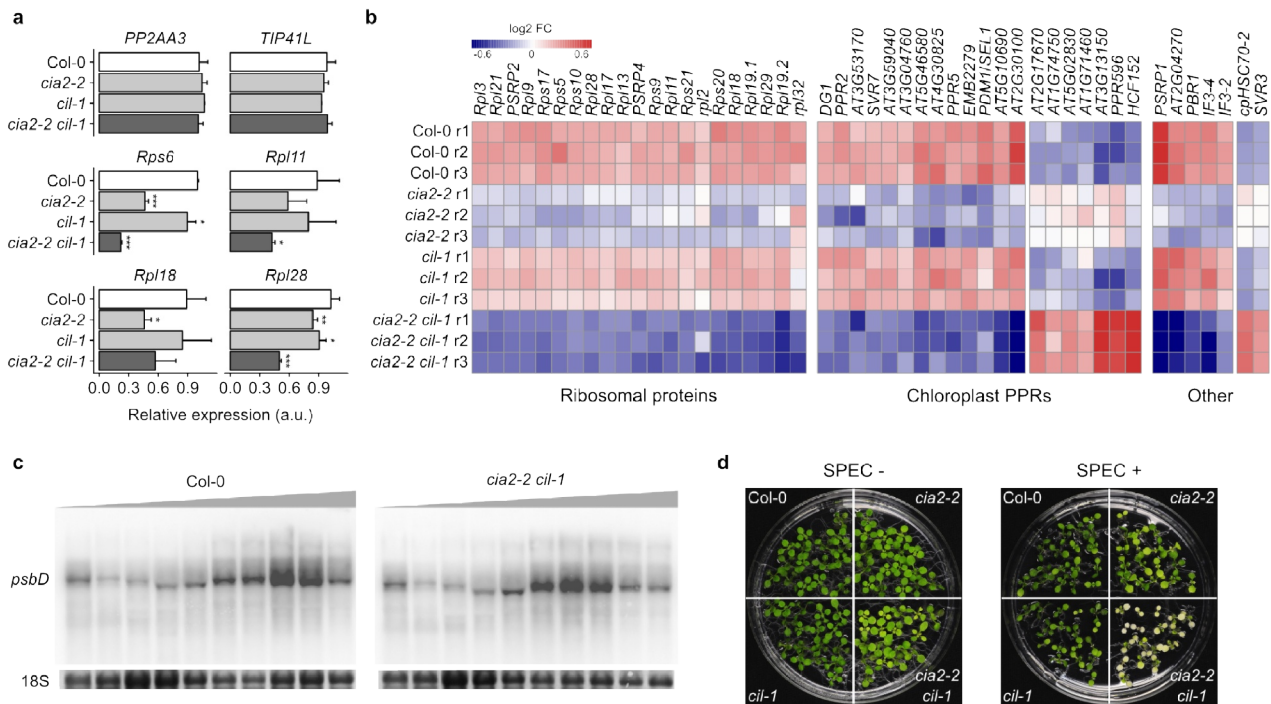


**Figure 5.** Characterization of chloroplast translation in analyzed genotypes. (a) Expression analysis of genes encoding chloroplast ribosomal proteins. Levels of analyzed transcripts were determined using qRT-PCR and normalized to two house-keeping genes (*PP2AA3* and *TIP41L*). Bars indicate mean values ± SD (three independent biological replicates). (b) Expression profile (RNA-seq) of genes involved in the regulation of plastid translation. (c) Polysome analysis reveals slower translation of *psbD* mRNA in *cia2-2 cil-1* double mutant as compared to Col-0. Gray triangles indicate the density of sucrose gradient. Methylene blue-stained 18S rRNA is shown as a loading control. (d) Susceptibility to chloroplast translation inhibitor (spectinomycin, 1.25 mg/L) of analyzed genotypes. Statistical significance (ANOVA and Tukey HSD test) is shown relative to Col-0 (\**p* < 0.05; \*\**p* < 0.01; \*\*\**p* < 0.001).



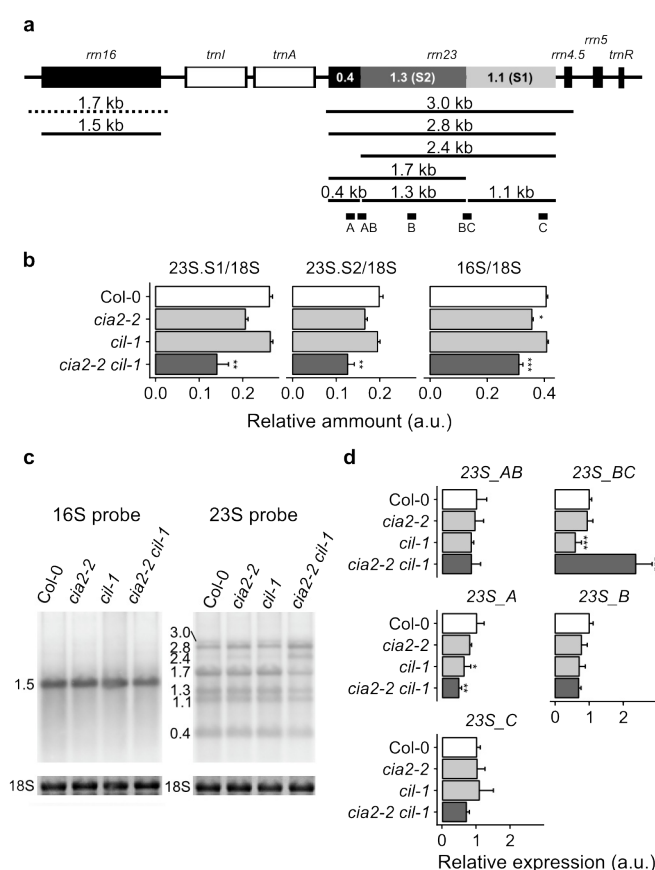


**Figure 6.** Maturation of plastid rRNAs. **(a)** Plastid rRNA operon. Mature forms of 16 and 23S rRNA are shown. Precursor of 23S rRNA is processed and cleaved into three parts: 0.4, 1.1, and 1.3 kb. **(b)** Relative abundance of precursor 23S and 16S rRNAs was measured using capillary electrophoresis and normalized to the cytoplasmic 18S rRNA. Values represent mean values  $\pm$  SEM ( $n = 3$ ). **(c)** Maturation and abundance of plastid rRNA were measured using Northern blot indicating that the 2.4 kb form of 23S rRNA is accumulated in *cia2-2 cil-1*. **(d)** Determination of relative amounts of 23S rRNA forms with qRT-PCR and primers (depicted in panel **(a)**) specific to each of cleaved fragments (primers A, B, and C) and flanking “hidden breaks” (primers AB and BC). Values were normalized to the level of 16S rRNA and represent mean values  $\pm$  SD ( $n = 3$ ). Statistical significance (ANOVA and Tukey HSD test) is shown relative to Col-0 (\* $p < 0.05$ ; \*\* $p < 0.01$ ; \*\*\* $p < 0.001$ ).



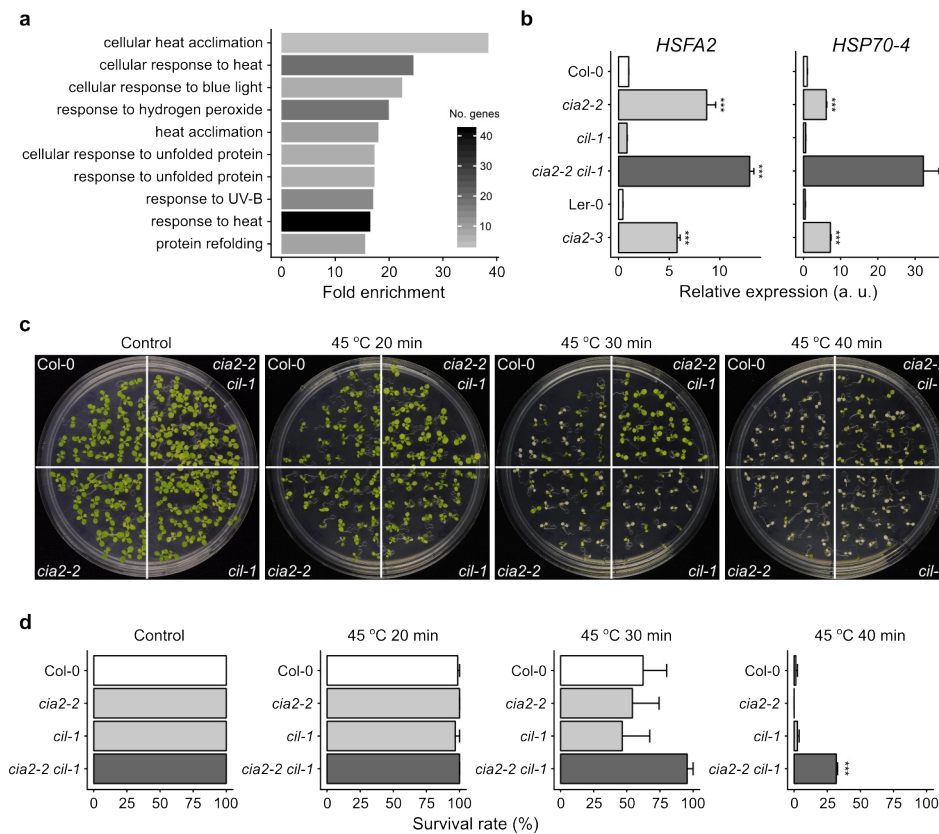


**Figure 7.** CIA2 and CIL negatively regulate tolerance to heat shock. **(a)** Gene ontology (GO) analysis of genes significantly induced in *cia2-2 cil-1* compared to Col-0 in the RNA-seq experiment. Ten most significantly overrepresented GO terms are shown. Number of genes in each group is shown in color of the bar. **(b)** Validation of expression of heat shock marker genes using qRT-PCR in analyzed genotypes and additional allele (*cia2-3*) in Ler-0 background (n = 3). Error bars represent  $\pm$  SD. **(c and d)** Thermo tolerance was tested in seedlings grown *in vitro*. Plants were exposed to 45 °C for a specific period of time. **(c)** Pictures of plants grown in control conditions 7 days after heat shock. **(d)** Survival rate of control and heat shock-treated plants. Error bars represent  $\pm$  SEM (n  $\geq$  3 plates) from two independent experiments (in total at least 75 seedlings were analyzed per genotype and treatment). Statistical significance (ANOVA and Tukey HSD test) is shown relative to corresponding WT (\*\*\*)  $p < 0.001$ .